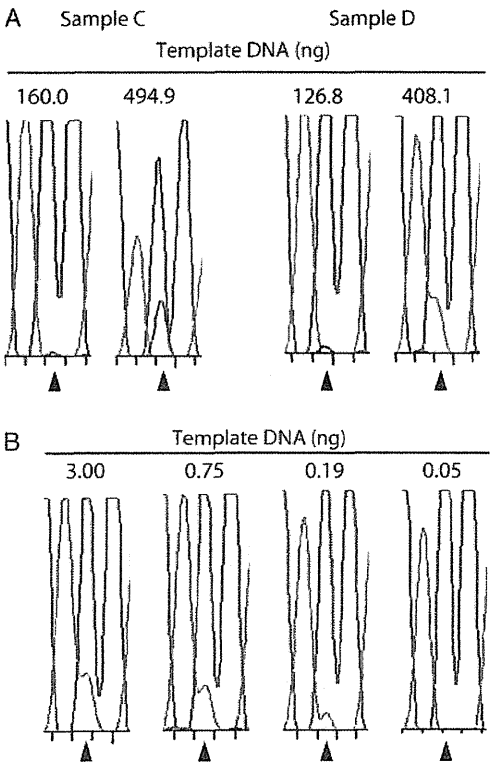

Figure 1. (A) Representative cases of conversion of wild-type to mutant signals. Analyzed data of antisense sequences of codon 12 of the *KRAS* gene for two samples are presented. Arrowheads represent the second letter of anticodon 12. Increase in the amount of the template DNA caused the occult peaks of T (red trace of sample C) and A (green trace of sample D) to become apparent. (B) Serial dilution of 10% mutation DNA and attenuation of the mutant signals. Analyzed data of antisense sequences of codon 12 of the *KRAS* gene for 10% mutation DNA models (37 cycles) are presented. Arrowheads represent the second letter of anticodon 12. As the amount of the template DNA was serially diluted to a quarter of the original and the total amount of DNA decreased, the mutant peak A diminished significantly or altogether disappeared.

DISCUSSION

ARMS/S is known to show a high sensitivity and specificity for the detection of *KRAS* mutations, with a short turnaround time. Meanwhile, DS is still recognized as one of the standard methods for mutation detection and is frequently used for confirming the results obtained with other methods. Comparisons of the sensitivity of the two methods have been reported. ARMS/S allows the detection of mutations in heterogeneous specimens, even at a low allelic concentration (1%), whereas DS allows the detection of heterogeneous mutant alleles present at 10–30%. Such difference in the sensitivity between the two methods has been regarded as the main reason for the discordance in the detection of *KRAS* mutations between the two methods (7,8,11).

In our present study, we showed that the discordance between the ARMS/S and DS for the detection of *KRAS* mutations was biased by the amount of amplifiable template DNA. Although the mutant-positive rates of ARMS/S and DS were not significantly different among samples with large DNA amounts, the mutant-positive rate of DS was significantly lower for samples with lower DNA amounts, suggesting that the discordance cannot be simply explained by the above-mentioned difference in the sensitivity between ARMS/S and DS. Subsequently performed experiments clearly showed that the sensitivity of DS was reduced by insufficient PCR amplification, which was caused not only by a lower template amount, but also by an inadequate number of PCR cycles.

To explain the above mechanism, a schematic model is presented in Fig. 2. Figure 2A represents the traces of the PCR-amplified copy numbers of the template containing three copies of mutant and seven copies of wild-type genes. The absolute copy numbers [(a) and (b) in Fig. 2A] increased exponentially by amplification. On the other hand, the fluorescent signals obtained by cycle sequencing of too small an amount of amplified DNA might not be detected by the capillary DNA sequencers. In this model, a copy number of 1024 is virtually designated as the detection threshold and the difference between the absolute copy numbers and the detection threshold is regarded as the 'detectable copy number' [(c) and (d) in Fig. 2A]. The detectable mutant/wild-type ratio [(c):(d) in Fig. 2A] supposedly represents the actual mutant/wild-type ratio. Throughout the amplification, the ratio of the absolute copy numbers of the mutant to wild-type DNA [(a):(b) in Fig. 2A] was fixed at 3:7; however, the detectable mutant/wild-type ratio was smaller when the absolute copy number was closer to the detection threshold. Figure 2B represents the change of the detectable mutant/wild-type ratio of 10% Mut DNA with a total 10, 100 and 1000 copies. The approximation of the detectable mutant/

Table 3. Alteration of the mutation/wild-type ratio of the *KRAS* gene in a mixture of 10% SW620 and 90% control genomic DNA (10% mutation DNA)

DNA amount (ng)	ARMS/S		Direct sequencing		
	Control C_t	ΔC_t	Mutant/wild-type ratio		
			35 cycles ($n = 3$)	37 cycles ($n = 5$)	40 cycles ($n = 5$)
3.00	30.73	2.84	0.225 ± 0.012	0.216 ± 0.010	0.242 ± 0.038
0.75	32.80	2.82	$0 \pm 0^{a,*}$	0.209 ± 0.053	0.230 ± 0.082
0.19	34.84	2.91	$0 \pm 0^{a,*}$	0.154 ± 0.108	0.237 ± 0.061
0.05	37.70	ND[b]	ND[b]	$0 \pm 0^{a,**}$	0.243 ± 0.214

[a]Wild-type signals could be detected, whereas mutant signals were not detectable.
[b]Neither wild-type nor mutant signals were detectable.
*Significantly different from the values in obtained with 40 cycles and 37 cycles of amplification of samples with an equivalent amount of DNA at $P < 0.05$ (ANOVA and Tukey's HSD procedure).
**Significantly different from the values obtained with 40 cycles in samples with an equivalent amount of DNA at $P < 0.05$ (ANOVA and Tukey's HSD procedure).

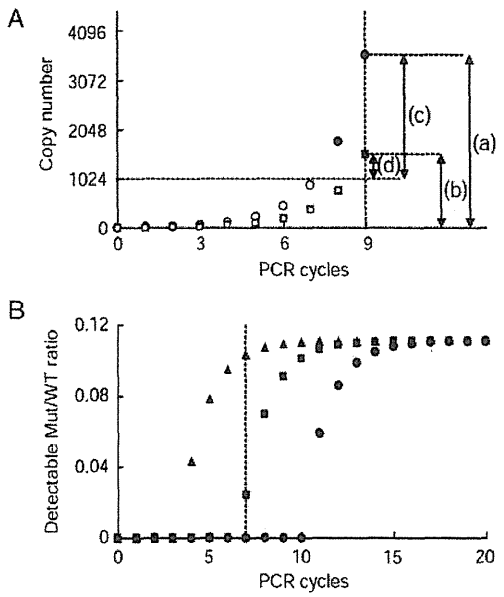

Figure 2. Schematic models of specific attenuation of the mutant signals. (A) Expected copy number of amplicons from a DNA template consisting of seven copies of the wild-type and three copies of the mutant genes. The copy number of 1024 was virtually designated as the detection threshold. Open circles, wild-type amplicons below the detection threshold; closed circles, wild-type amplicons over the detection threshold; open squares, mutant amplicons below the detection threshold; closed squares, mutant amplicons over the detection threshold. (a) and (b): absolute copy number of the wild-type and mutant amplicons, respectively. (c) and (d): detectable copy number of the wild-type and mutant amplicons, respectively. (B) The change of the detectable mutation/wild-type ratio obtained for 10% Mut DNA with a total of 10 (closed circles), 100 (closed squares) and 1000 (closed triangles) copies. WT, wild-type.

wild-type ratio to the absolute mutant/wild-type ratio was delayed when the initial copy number was small. At the seventh PCR cycle, the detectable mutant/wild-type ratio for the 10-, 100- and 1000-copy models were 0, 0.024 and 0.103, respectively. This model also suggests that even with a small initial copy number, the detectable mutant/wild-type ratio approximated the absolute mutant/wild-type ratio when the PCR amplification efficiently amplified the DNA to levels high enough to overshadow the detection threshold. The results obtained with these models are consistent with our finding of the loss of mutant signals in samples containing lower amounts of template DNA or obtained using a smaller number of amplification cycle.

Amplifiable DNA amounts are often limited when FFPE samples are used as the DNA source, since DNA is highly fragmented by formalin treatment. Previous studies have emphasized the harmful effects of fixatives on the efficiency of amplification by PCR. Especially, prolonged fixation periods contribute to further deterioration of the template DNA (13,14). Standardization of the conditions of formalin fixation is, without doubt, important to improve the quality of any DNA testing. However, at present, we have to use archived FFPE samples with various fixation conditions in routine clinical testing. In this study, we tried to obtain detailed data about the fixation conditions; however, the information was not recorded for many of the samples, especially those from other hospitals, and we could not conduct the evaluation in the present study.

To ensure the robustness of DS, it is necessary to set the appropriate conditions for PCR amplification from samples with low-quality DNA. Since various laboratories have established 'home-brewed' DS methods, it is difficult to propose a single standard method that can be demonstrated to be superior to other established methods. Regardless of specific conditions, such as the primer sequences, sizes of the PCR products and brands of DNA polymerases and thermal cyclers, we strongly recommend confirmation of whether the PCR amplification is saturated before the start of cycle sequencing. According to our experimental results, PCR conditions amplifying 0.05 ng of intact genomic DNA, which is equivalent to tens of haploid copies, to saturation level might be required. Since the amplifiable amount of DNA from FFPE specimens is often limited, increase in the number of PCR cycles (more than 40 cycles) may be most effective. The potential risk of detection of artificial mutations with the use of insufficient amounts of the template DNA from FFPE specimens and increased number of PCR cycles has been suggested (15); to avoid such false-positive errors, duplication of the test would be expected to be effective.

Genetic tests for appropriate use of molecular-targeting drugs are becoming increasingly popular and necessary. In many cases, DS will be the primary procedure for the detection of gene mutations in DNA samples from FFPE specimens. As suggested above, validation of the testing conditions, including the PCR settings, would be most required to strengthen the robustness and rigidity of the tests for routine clinical diagnoses.

Funding

H.E. was supported by Grants for the Third-Term Comprehensive 10-Year Strategy for Cancer Control, a Grant-in-Aid for Cancer Research from the Ministry of Health, Labour and Welfare and a Grant-in-Aid for Scientific Research on Priority Areas from the Ministry of Education, Culture, Sports, Science and Technology, Japan. T.Y. and K.T. were supported by a Grant-in-Aid for Cancer Research from the Ministry of Health, Labour and Welfare, Japan.

Conflict of interest statement

None declared.

References

1. Karapetis CS, Khambata-Ford S, Jonker DJ, O'Callaghan CJ, Tu D, Tebbutt NC, et al. K-ras mutations and benefit from cetuximab in advanced colorectal cancer. *N Engl J Med* 2008;359:1757–65.

2. Van Cutsem E, Kohne CH, Hitre E, Zaluski J, Chang Chien CR, Makhson A, et al. Cetuximab and chemotherapy as initial treatment for metastatic colorectal cancer. *N Engl J Med* 2009;360:1408–17.
3. Amado RG, Wolf M, Peeters M, Van Cutsem E, Siena S, Freeman DJ, et al. Wild-type KRAS is required for panitumumab efficacy in patients with metastatic colorectal cancer. *J Clin Oncol* 2008;26:1626–34.
4. Tol J, Koopman M, Cats A, Rodenburg CJ, Creemers GJ, Schrama JG, et al. Chemotherapy, bevacizumab, and cetuximab in metastatic colorectal cancer. *N Engl J Med* 2009;360:563–72.
5. Newton CR, Graham A, Heptinstall LE, Powell SJ, Summers C, Kalsheker N, et al. Analysis of any point mutation in DNA. The amplification refractory mutation system (ARMS). *Nucleic Acids Res* 1989;17:2503–16.
6. Whitcombe D, Theaker J, Guy SP, Brown T, Little S. Detection of PCR products using self-probing amplicons and fluorescence. *Nat Biotechnol* 1999;17:804–7.
7. Kotoula V, Charalambous E, Biesmans B, Malousi A, Vrettou E, Fountzilas G, et al. Targeted KRAS mutation assessment on patient tumor histologic material in real time diagnostics. *PLoS ONE* 2009;4:e7746.
8. Franklin WA, Haney J, Sugita M, Bemis L, Jimeno A, Messersmith WA. KRAS mutation: comparison of testing methods and tissue sampling techniques in colon cancer. *J Mol Diagn* 2009;12:43–50.
9. Ogasawara N, Bando H, Kawamoto Y, Yoshino T, Tsuchihara K, Ohtsu A, et al. Feasibility and robustness of amplification refractory mutation system (ARMS)-based KRAS testing using clinically available formalin-fixed, paraffin-embedded samples of colorectal cancers. *Jpn J Clin Oncol* 2010; doi:10.1093/jjco/hyq151 (Epub ahead of print).
10. Jimeno A, Messersmith WA, Hirsch FR, Franklin WA, Eckhardt SG. KRAS mutations and sensitivity to epidermal growth factor receptor inhibitors in colorectal cancer: practical application of patient selection. *J Clin Oncol* 2009;27:1130–6.
11. Angulo B, Garcia-Garcia E, Martinez R, Suarez-Gauthier A, Conde E, Hidalgo M, et al. A commercial real-time PCR kit provides greater sensitivity than direct sequencing to detect KRAS mutations: a morphology-based approach in colorectal carcinoma. *J Mol Diagn* 2010;12:292–9.
12. Shigematsu H, Lin L, Takahashi T, Nomura M, Suzuki M, Wistuba II, et al. Clinical and biological features associated with epidermal growth factor receptor gene mutations in lung cancers. *J Natl Cancer Inst* 2005;97:339–46.
13. Srinivasan M, Sedmak D, Jewell S. Effect of fixatives and tissue processing on the content and integrity of nucleic acids. *Am J Pathol* 2002;161:1961–71.
14. Yokota T, Shibata N, Ura T, Takahari D, Shitara K, Muro K, et al. Cycleave polymerase chain reaction method is practically applicable for V-Ki-ras2 Kirsten rat sarcoma viral oncogene homolog (KRAS)/V-raf murine sarcoma viral oncogene homolog B1 (BRAF) genotyping in colorectal cancer. *Transl Res* 2010;156:98–105.
15. Williams C, Ponten F, Moberg C, Soderkvist P, Uhlen M, Ponten J, et al. A high frequency of sequence alterations is due to formalin fixation of archival specimens. *Am J Pathol* 1999;155:1467–71.

JJCO Japanese Journal of Clinical Oncology

Jpn J Clin Oncol 2011;41(1)52–56
doi:10.1093/jjco/hyq151
Advance Access Publication 9 August 2010

Feasibility and Robustness of Amplification Refractory Mutation System (ARMS)-based *KRAS* Testing Using Clinically Available Formalin-fixed, Paraffin-embedded Samples of Colorectal Cancers

Naomi Ogasawara[1], Hideaki Bando[2], Yasuyuki Kawamoto[2], Takayuki Yoshino[2], Katsuya Tsuchihara[1], Atsushi Ohtsu[2] and Hiroyasu Esumi[1,*]

[1]Cancer Physiology Project, Research Center for Innovative Oncology, National Cancer Center Hospital East, Kashiwa, Japan and [2]Division of Gastrointestinal Oncology, National Cancer Center Hospital East, Kashiwa, Japan

*For reprints and all correspondence: Hiroyasu Esumi, National Cancer Center Hospital East, 6-5-1 Kashiwanoha, Kashiwa, Chiba 277-8577, Japan. E-mail: hesumi@east.ncc.go.jp

Received May 25, 2010; accepted July 10, 2010

Background: *KRAS* mutation testing is recommended for the discernment of metastatic colorectal cancer patients who are unlikely to benefit from anti-epidermal growth factor receptor antibodies. A recently developed amplification refractory mutation-Scorpion system is becoming a standard method for *KRAS* mutant detection. The feasibility and robustness of this system using DNA samples from clinically available formalin-fixed, paraffin-embedded specimens were evaluated.

Methods: Genomic DNA from macro-dissected 110 specimens was applied for the *KRAS* mutant detection using a commercial amplification refractory mutation-Scorpion system kit. Success rate and mutant detection rate of the test were evaluated.

Results: Small intra- and inter-lot deviations of the testing kit and a good concordance among different real-time polymerase chain reaction systems suggested the reliability of the amplification refractory mutation-Scorpion system. Though one-third of the 110 samples that were tested did not contain a sufficient amount of DNA to detect a 1% concentration of mutant alleles, the mutant detection rate was not impaired using tumor DNA concentrated by macro-dissection. Using a higher amount of template DNA, which supposedly contained abundant interfering substances, prevented the detection of the exogenous control amplicons, resulting in a reduced success rate. Adjusting the template amount according to the total DNA concentration might reduce the failure rate.

Conclusion: The amplification refractory mutation-Scorpion system with formalin-fixed, paraffin-embedded specimen-derived DNA samples exhibited an acceptable feasibility and robustness suitable for routine clinical practice.

Key words: colorectal cancer – KRAS mutation – ARMS-Scorpion method – FFPE

INTRODUCTION

The clinical benefits of anti-EGFR (epidermal growth factor receptor) antibodies for the treatment of metastatic colorectal cancer (mCRC) have been revealed in randomized clinical trials (1–3). Meanwhile, retrospective subset analyses of these trials have clarified that patients with tumors containing mutant *KRAS* genes, which encode constitutively active forms of KRAS proteins, did not benefit from anti-EGFR antibodies. Based on this evidence, *KRAS* mutation testing is now strongly recommended prior to the use of anti-EGFR antibodies (4,5).

A series of procedures have been developed for detecting *KRAS* mutations in genomic DNA from archived formalin-fixed, paraffin-embedded (FFPE) specimens. Among them, a recently developed mutation-specific real-time polymerase chain reaction (PCR)-based technique, combining an amplification refractory mutation system and a Scorpion fluorescent primer/probe system (ARMS/

S), offers both simple and rapid means of testing (6,7). A single kit detects seven major mutations in codons 12 and 13 of the *KRAS* gene in heterogeneous specimens at a low allelic concentration (1%), with detection limits of between 5 and 10 copies. This assay has been used in several phase III trials examining the use of anti-EGFR antibody treatment in patients with mCRC, and a commercialized, quality-controlled kit has been approved for the CE mark, indicating conformity with European health and safety requirements (4,8).

Though the ARMS/S method is likely to be a valuable tool in clinical practice, the feasibility and robustness of this system using DNA samples from clinically available FFPE specimens have not been well evaluated. In the present study, we explored the feasibility and robustness of this kit and the DNA properties that influence a successful test outcome.

PATIENTS AND METHODS

Tissue Samples and DNA Extraction

Samples from 110 mCRC patients who were planned to receive anti-EGFR antibody treatment between April and November 2009 were available for *KRAS* mutation testing. The test was performed as a part of the Advanced Medical Technology Programs approved by the Ministry of Health, Labour and Welfare of Japan and written informed consent was obtained from all the patients. All the specimens had been obtained from primary or metastatic tumors collected by surgical resection or biopsy. Genomic DNA was isolated from FFPE tissue blocks using the QIAamp DNA FFPE Tissue Kit (QIAGEN) according to the manufacturer's instructions. To enrich the tumor-derived DNA, the tissue areas containing more than 70% tumor cells from each section were macro-dissected. The extracted DNA was spectrophotometrically quantified using Nano Drop 1000 (Thermo Fischer Scientific).

KRAS Mutant Detection

Mutant *KRAS* was determined using the K-RAS Mutation Test Kit (DxS-QIAGEN) according to the manufacturer's instructions. Real-time PCR was performed and analyzed using the LightCycler 480 Real-Time PCR System and LightCycler Adapt software v1.1 (Roche Diagnostics) or the 7500 Fast Real-Time PCR System (Applied Biosystems-Life Technologies).

RESULTS

Negligible Intra- and Inter-lot Differences Obtained with the K-RAS Mutation Kit

To evaluate the deviation in the data among each run, we estimated the Ct (cycle threshold) values for the amplification plots of the kit-attached mixed standard. The mixed standard contains all the mutant fragments. Amplification with a control, which amplifies a region of exon 4 of *KRAS*, and 7 mutant-specific primers provided constant Ct values. Using three different lots of the kit, a total of 27 runs were performed using the Roche LightCycler 480 Real-Time PCR System (LC480). All the plots exhibited the Ct values of the control and mutation assays with a small standard deviation (SD), and these values converged within the range reported by the manufacturer. The differences in the Ct values among the different lots were also negligible (Figure 1 and Table 1).

Good Concordance between Recommended Real-Time PCR Systems

Two real-time PCR systems, the LC480 mentioned above and the Applied Biosystems 7500 Real-Time PCR System (ABI7500), have been approved for *in vitro* diagnostic use in Europe. The deviation in the results obtained using these two systems was assessed. Eleven randomly selected samples that were identified as mutation positive using the LC480 system were re-tested using the ABI7500 system. All the mutation callings were concordant between two systems. Furthermore, once the threshold of the ABI7500 system was adjusted so that it was equal to the control Ct value of the mixed standard identified using the LC480 system, the differences in the control Ct values of the samples became very small (mean and SD, -0.55 ± 0.83). The differences in ΔCt (the difference between the mutation assay Ct and the control assay Ct) between the two systems were also significantly small (mean and SD, 0.20 ± 1.31). Confirmatory direct sequencing did not detect any mutant signals in 4 of the 11 samples, however the other mutation interpretations were concordant with those obtained using the ARMS-Scorpion kit (Table 2).

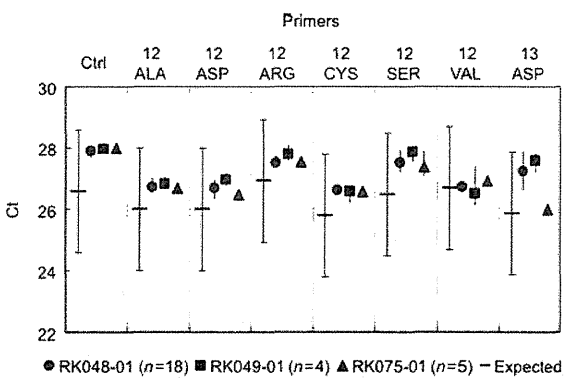

Figure 1. Intra- and inter-lot differences of the tests. The means and ranges of the Ct values for the amplification plots of the mixed standard produced using a total of 27 runs with three different lots were plotted. The expected Ct values and permissible ranges provided by the manufacturer were also plotted.

Table 1. Intra- and inter-lot differences of the test

Primer	Lot	*n*	Ct		Range	
			Mean	SD	Upper	Lower
	RK048-01	18	27.90	0.10	28.09	27.70
Control	RK049-01	4	27.98	0.13	28.21	27.89
	RK075-01	5	28.01	0.04	28.05	27.94
	RK048-01	18	26.73	0.17	27.04	26.52
12ALA	RK049-01	4	26.81	0.15	27.06	26.64
	RK075-01	5	26.68	0.12	26.88	26.52
	RK048-01	18	26.69	0.16	26.98	26.36
12ASP	RK049-01	4	26.97	0.18	27.21	26.71
	RK075-01	5	26.47	0.12	26.64	26.28
	RK048-01	18	27.52	0.09	27.72	27.34
12ARG	RK049-01	4	27.79	0.20	28.09	27.55
	RK075-01	5	27.56	0.06	27.63	27.49
	RK048-01	18	26.62	0.08	26.81	26.49
12CYS	RK049-01	4	26.59	0.24	26.78	26.20
	RK075-01	5	26.60	0.10	26.77	26.50
	RK048-01	18	27.52	0.20	27.94	27.20
12SER	RK049-01	4	27.85	0.21	28.10	27.54
	RK075-01	5	27.38	0.30	27.90	27.07
	RK048-01	18	26.72	0.10	26.92	26.55
12VAL	RK049-01	4	26.53	0.50	27.40	26.15
	RK075-01	5	27.38	0.09	27.08	26.81
	RK048-01	18	27.24	0.39	27.88	26.53
13ASP	RK049-01	4	27.57	0.26	27.85	27.20
	RK075-01	5	25.99	0.12	26.19	25.84

Limits of Sample Assessment Interpretation

LightCycler Adapt Software is recommended for the analysis of data obtained using the LC480 system. The software calculates the sample ΔCt values, which are compared with the cut-off values for a 1% concentration of mutant alleles, to identify a positive or negative amplification plot. A CONF_LEVEL Flag/Warning is displayed in a mutation-negative sample with a control Ct > 28.9, suggesting the absence of an amount of amplifiable DNA sufficient to detect a 1% mutation and indicating that low-level mutations might have been missed. As well, a LIMITED Flag/Warning is displayed in a mutation-negative sample with a control Ct >35 to warn that the system has only detected apparent mutations. Of the 110 samples that were tested, 35 samples (31.8%) were judged as CONF_LEVEL and three samples (2.7%) were judged as LIMITED (Fig. 2). However, the mutant detection rates of the samples with a control Ct below and above 28.9 were 40.9 and 40.0%, respectively (Fig. 2).

Exogenous Control Failure Using a Larger Amount of DNA Templates

The assays contain an exogenous control reaction to assess contamination with PCR inhibitors. If the exogenous control reactions fail and no mutant-specific amplification was detected, an EXO_FAIL Flag/Warning is displayed. EXO_FAIL warnings were displayed in 25 of the 110 samples (22.7%) that were examined. All the samples were mapped onto a two-dimensional plot with the control Ct value and the spectrophotometrically determined gross amount of DNA used in the reaction. The EXO_FAIL samples converged within an area corresponding to a larger amount of DNA and smaller Ct values. The lowest DNA

Table 2. Concordance between runs performed using different real-time PCR systems

Sample	LC480			7500 Fast			dCt (LC480-7500)	ddCt (LC480-7500)	DS interpretation
	Ct	dCt	Interpretation	Ct	dCt	Interpretation			
A	26.69	4.71	12Cys	26.98	2.02	12Cys	−0.29	2.69	12Cys
B	28.64	0.16	12Val	30.93	0.81	12Val	−2.29	−0.65	12Val
C	30.32	2.48	12Cys	31.04	1.80	12Cys	−0.66	0.68	12Cys
D	31.32	3.52	12Ala	32.37	3.69	12Ala	−1.05	−0.17	WT
E	31.50	3.63	12Asp	32.93	2.95	12Asp	−1.43	0.68	12Asp
F	31.72	6.61	13Asp	32.50	3.64	13Asp	−0.78	2.52	13Asp
G	31.83	3.40	12Cys	31.11	4.20	12Cys	0.72	−0.80	WT
H	32.37	0.34	12Ala	33.01	1.04	12Ala	−0.64	−0.70	12Ala
I	32.55	6.36	12Cys	32.76	6.64	12Cys	−0.21	−0.28	WT
J	32.79	2.92	12Val	32.21	4.72	12Val	0.58	−1.80	WT
K	32.96	2.17	12ASP	32.93	2.13	12Asp	0.03	0.04	12Asp

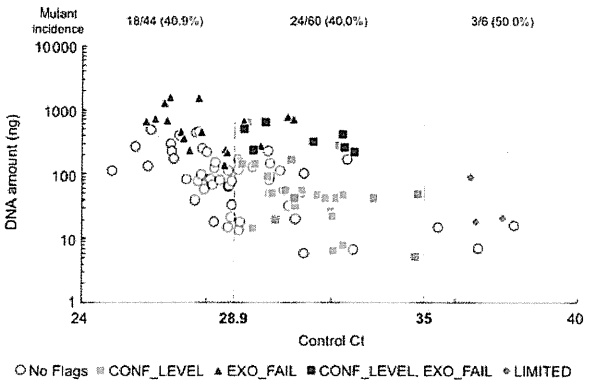

Figure 2. DNA amount and sample assessment interpretation. The spectrophotometrically determined DNA amounts used for the single assay and control Ct values of each sample were plotted. Control Ct values of 28.9 and 35 were used as the cut-off values for CONF_LEVEL and LIMITED warnings, respectively. The Flag/Warning results were overlaid on the plot. The incidence of the mutation was indicated above the plot. The results were stratified according to the control Ct values.

amount and the largest Ct value for the EXO_FAIL samples were 139.2 ng per reaction and 32.71, respectively. The number of mutation-negative samples with more than 139.2 ng of DNA was 27, i.e. the incidence of the EXO_FAIL warning was 92.6% (25/27). Meanwhile, the number of mutation-negative samples with a Ct value of less than 32.71 was 59, i.e. the incidence of the EXO_FAIL warning was 42.4% (25/59, Fig. 2).

DISCUSSION

One of the advantages of the ARMS/S system for *KRAS* testing is its expediency for standardizing operating procedures. The significantly small intra- and inter-lot deviations obtained in the present study suggest the reliability of the meta-chronically obtained data. Furthermore, the good concordance between different real-time PCR systems assures consistency among different facilities.

The limited amount of DNA in archived samples, mainly caused by fragmentation as a result of formalin treatment, often makes *KRAS* testing difficult using FFPE samples (9). Though the standardization of the fixation methods, such as concentration and pH of formalin and fixation time, is highly recommended, controlling these factors of clinically available archived samples is quite difficult. Actually, we could not follow the information of fixation methods of most of the specimens examined in this study, and about one-third of the samples did not satisfy the criteria for assuring sensitivity capable of detecting a 1% mutation rate. However, the mutation incidences were similar between the samples with a control Ct below and above 28.9, suggesting that the limited sensitivity did not lower the detection power, at least using DNA samples that had been enriched by macro-dissection.

In addition to its high sensitivity, robustness is another advantage of ARMS/S system. Discordant mutant interpretation between ARMS/S and direct sequencing was observed in 4 of 11 samples. All the four samples exhibited the control Ct value >28.9, suggesting that the amplifiable DNA amount of these samples was rather limited. Using a larger sample size, we confirmed a similar phenomenon and found that the sensitivity of direct sequencing was impaired by insufficient template DNA amount, resulting false-negative results for mutant detection (Bando, submitted for publication). Taking different sensitivity and robustness into account, which testing method, ARMS/S or direct sequencing, provides better conformity to the clinical benefit of anti-EGFR antibodies should be further investigated.

Unamplifiable DNA and other contaminants can interfere with PCR-based assays. The results showing that EXO_FAIL warnings were observed among the samples with larger amounts of DNA supports this idea. A threshold determined by the amount of total DNA might be useful to reduce the appearance of EXO_FAIL warnings, compared with a threshold determined by the control Ct value. Theoretically, the control Ct stands for the amount of amplifiable DNA, while the spectrophotometrically determined DNA amount reflects the sum of the amplifiable and unamplifiable DNA. Thus, the above finding seems to suggest that the total DNA concentration is correlated with the incidence of EXO_FAIL warnings. The manufacturer's instruction suggests repeating the assays using diluted DNA samples if this warning appears. In such cases, checking the total amount of DNA, rather than the control Ct of the primary assays, might produce better results. However, DNA dilution sometimes causes a trade-off between a decreasing EXO_FAIL incidence and a decreasing sensitivity. Limited DNA yields from clinical specimens can be quite troublesome in such cases. Improving the quality of DNA samples, for example, by eliminating necrotic tissues and the remains of hemorrhage during macro-dissection, the use of alternative DNA extraction methods that do not require spin-columns or filtering out contaminants with lower molecular weights might help to resolve this problem.

In conclusion, ARMS/S testing using FFPE-derived DNA samples exhibited a good feasibility and robustness that might satisfy the requirements for routine clinical practice. To maintain the reliability of this test, authorized quality assurance/control programs for laboratories should be required, and the merits and demerits of this system versus other *KRAS* mutation tests will need to be further evaluated in clinical use.

Funding

This work was supported by a grant for the Third-Term Comprehensive 10-Year Strategy for Cancer Control from the Ministry of Health, Labour and Welfare [H22-3ji taigann-ippann-033 to H.E] and a grant-in-aid for cancer research from the Ministry of Health, Labour and Welfare [21bunn-shi-4–5 to K.T, T.Y].

Conflict of interest statement

None declared.

References

1. Cunningham D, Humblet Y, Siena S, Khayat D, Bleiberg H, Santoro A, et al. Cetuximab monotherapy and cetuximab plus irinotecan in irinotecan-refractory metastatic colorectal cancer. *N Engl J Med* 2004;351:337–45.
2. Jonker DJ, O'Callaghan CJ, Karapetis CS, Zalcberg JR, Tu D, Au HJ, et al. Cetuximab for the treatment of colorectal cancer. *N Engl J Med* 2007;357:2040–8.
3. Van Cutsem E, Peeters M, Siena S, Humblet Y, Hendlisz A, Neyns B, et al. Open-label phase III trial of panitumumab plus best supportive care compared with best supportive care alone in patients with chemotherapy-refractory metastatic colorectal cancer. *J Clin Oncol* 2007;25:1658–64.
4. Amado RG, Wolf M, Peeters M, Van Cutsem E, Siena S, Freeman DJ, et al. Wild-type KRAS is required for panitumumab efficacy in patients with metastatic colorectal cancer. *J Clin Oncol* 2008;26:1626–34.
5. Karapetis CS, Khambata-Ford S, Jonker DJ, O'Callaghan CJ, Tu D, Tebbutt NC, et al. K-ras mutations and benefit from cetuximab in advanced colorectal cancer. *N Engl J Med* 2008;359:1757–65.
6. Newton CR, Graham A, Heptinstall LE, Powell SJ, Summers C, Kalsheker N, et al. Analysis of any point mutation in DNA. The amplification refractory mutation system (ARMS). *Nucleic Acids Res* 1989;17:2503–16.
7. Whitcombe D, Theaker J, Guy SP, Brown T, Little S. Detection of PCR products using self-probing amplicons and fluorescence. *Nat Biotechnol* 1999;17:804–7.
8. Tol J, Koopman M, Cats A, Rodenburg CJ, Creemers GJ, Schrama JG, et al. Chemotherapy, bevacizumab, and cetuximab in metastatic colorectal cancer. *N Engl J Med* 2009;360:563–72.
9. Williams C, Pontén F, Moberg C, Söderkvist P, Uhlén M, Pontén J, et al. A high frequency of sequence alterations is due to formalin fixation of archival specimens. *Am J Pathol* 1999;155:1467–71.

Sucrose nonfermenting AMPK-related kinase (SNARK) mediates contraction-stimulated glucose transport in mouse skeletal muscle

Ho-Jin Koh[a], Taro Toyoda[a], Nobuharu Fujii[a,1], Michelle M. Jung[a], Amee Rathod[a], R. Jan-Willem Middelbeek[a], Sarah J. Lessard[a], Jonas T. Treebak[b], Katsuya Tsuchihara[c], Hiroyasu Esumi[c], Erik A. Richter[b], Jørgen F. P. Wojtaszewski[b], Michael F. Hirshman[a], and Laurie J. Goodyear[a,2]

[a]Research Division, Joslin Diabetes Center and Department of Medicine, Harvard Medical School, Boston, MA 02215; [b]Molecular Physiology Group, Copenhagen Muscle Research Centre, Department of Exercise and Sport Sciences, University of Copenhagen, DK-2100 Copenhagen, Denmark; and [c]Cancer Physiology Project, Research Center for Innovative Oncology, National Cancer Center Hospital East, Kashiwa, Chiba 277-8577, Japan

Communicated by C. Ronald Kahn, Joslin Diabetes Center, Boston, MA, June 29, 2010 (received for review December 22, 2009)

The signaling mechanisms that mediate the important effects of contraction to increase glucose transport in skeletal muscle are not well understood, but are known to occur through an insulin-independent mechanism. Muscle-specific knockout of LKB1, an upstream kinase for AMPK and AMPK-related protein kinases, significantly inhibited contraction-stimulated glucose transport. This finding, in conjunction with previous studies of ablated AMPKα2 activity showing no effect on contraction-stimulated glucose transport, suggests that one or more AMPK-related protein kinases are important for this process. Muscle contraction increased sucrose nonfermenting AMPK-related kinase (SNARK) activity, an effect blunted in the muscle-specific LKB1 knockout mice. Expression of a mutant SNARK in mouse tibialis anterior muscle impaired contraction-stimulated, but not insulin-stimulated, glucose transport. Whole-body SNARK heterozygotic knockout mice also had impaired contraction-stimulated glucose transport in skeletal muscle, and knockdown of SNARK in C2C12 muscle cells impaired sorbitol-stimulated glucose transport. SNARK is activated by muscle contraction and is a unique mediator of contraction-stimulated glucose transport in skeletal muscle.

LKB1 | Akt Substrate of 160 kDa | TBC1D1 | exercise

It has long been known that physical exercise has important benefits for people with type 2 diabetes, due in part to the increased rates of glucose transport and enhanced insulin sensitivity of the contracting skeletal muscles. Given the importance of exercise in regulating glucose homeostasis, it is not surprising that during the past decade there has been extensive research focused on establishing the signaling pathways that regulate exercise-stimulated glucose transport in skeletal muscle. Early data showed that there are different mechanisms for the stimulation of glucose transport by exercise and insulin, because the combination of a maximal insulin stimulus plus a maximal contraction stimulus has additive or partially additive effects on glucose transport (1–3). It has also been established by several groups that there are distinct proximal signals leading to glucose transport by insulin and exercise in skeletal muscle (4–10). Although the mechanism for insulin-stimulated glucose transport is fairly well understood, elucidating the signals that mediate contraction-stimulated glucose transport has proven to be a challenging task. Several reports have suggested the involvement of the LKB1/AMP-activated protein kinase (AMPK) signaling axis as a central player in contraction-stimulated glucose transport in skeletal muscle (4, 11, 12).

LKB1 is a Ser/Thr kinase that was originally identified as a tumor suppressor protein, and is now known to be a critical regulator of metabolism in liver and skeletal muscle (12–14). LKB1 functions as a kinase in a complex with the two regulatory subunits, STE20-related kinase adaptor (STRAD) and mouse protein 25 (MO25). This complex phosphorylates AMPK as well as at least 12 of the AMPK-related kinases (15, 16). There is limited knowledge of the function of most of the AMPK-related protein kinases, with the exception of AMPK. AMPK has emerged as a master metabolic signaling protein, regulating cellular metabolism not only in skeletal muscle but in many other tissues (17–19). In skeletal muscle, AMPK is necessary for the increase in glucose transport in response to some insulin-independent stimuli, such as 5-aminoimidazole-4-carboxamide ribonucleoside (AICAR) (20–22) and hypoxia (20). However, through the use of knockout and transgenic approaches, it is now clear that AMPK cannot be the sole regulator of contraction-stimulated glucose transport (20–23).

Sucrose nonfermenting AMPK-related kinase (SNARK/NUAK2) was identified in 2001 as the fourth member of the AMPK family of kinases (24). The catalytic domain of SNARK has significant homology with the catalytic domains of AMPKα1 (46%), AMPKα2 (41%), and the AMPK-related kinase 5 (ARK5; 55%), whereas the C terminus is not conserved with other AMPK family members. LKB1 phosphorylates SNARK at Thr^{208}, increasing SNARK activity by 50-fold in vitro (16). Little is known about SNARK function, although AICAR and cellular stressors such as glucose deprivation, rotenone, and sorbitol have been reported to increase SNARK activity in multiple cell-culture lines (24–26). Whole-body SNARK heterozygotic knockout $^{(+/-)}$ mice were recently generated and showed increased body weights, increased fat mass, and fatty livers in response to 8 wk of treatment with the carcinogenic compound azoxymethane (27). The mice also displayed increased serum triglyceride concentrations, hyperinsulinemia, hyperglycemia, and glucose intolerance (27), suggesting the possibility that SNARK functions in the regulation of glucose and lipid homeostasis. However, a recent report has shown no effect of knockdown of SNARK in regulating insulin-stimulated glucose transport in human primary myotubes (28).

In the present study, we found that muscle-specific LKB1 knockout mice (MLKB1KO), which have ablated AMPKα2 activity, had a significant reduction in contraction-stimulated glucose transport. Because we previously showed that AMPKα2 inactive mice have normal contraction-stimulated glucose transport (20), this suggests that one or more additional LKB1 substrates must be involved in the regulation of contraction-stimulated glucose transport. In investigating the AMPK-related protein kinases, we found that contraction in situ increased SNARK activity in the skeletal muscles of control mice, and that this increase was abolished in MLKB1KO mice. Contraction of isolated mouse skeletal

Author contributions: H.-J.K., N.F., and L.J.G. designed research; H.-J.K., T.T., N.F., M.M.J., A.R., R.J.-W.M., S.J.L., J.T.T., and M.F.H. performed research; J.T.T., K.T., H.E., E.A.R., and J.F.P.W. contributed new reagents/analytic tools; H.-J.K., T.T., N.F., M.F.H., and L.J.G. analyzed data; and H.-J.K. and L.J.G. wrote the paper.

The authors declare no conflict of interest.

[1]Present address: Department of Health Promotion Sciences, Tokyo Metropolitan University, Tokyo 192-0397, Japan.

[2]To whom correspondence should be addressed. E-mail: laurie.goodyear@joslin.harvard.edu.

This article contains supporting information online at www.pnas.org/lookup/suppl/doi:10.1073/pnas.1008131107/-/DCSupplemental.

muscles in vitro, as well as exercise in vivo in mice and humans, also increased SNARK activity in skeletal muscle. Furthermore, we investigated the potential role of SNARK in contraction-stimulated glucose transport in skeletal muscle.

Results

LKB1 Regulates Contraction-Stimulated Glucose Transport. We have previously reported that MLKB1KO mice have a 95% reduction in LKB1 protein in skeletal muscle and ablation of AMPKα2 activity in this tissue (13). To investigate the role of skeletal muscle LKB1 in contraction-stimulated glucose transport, isolated soleus muscles from control and MLKB1KO mice were contracted by electrical stimulation for 10 min, and glucose transport was measured using radioactive tracers. There was no difference in basal glucose transport between control and MLKB1KO mice (Fig. 1*A*). Similar to a previous study where a hypomorphic LKB1 knockout mouse was studied (12), contraction increased glucose transport in control mice, and this was significantly decreased by ≈40% in the MLKB1KO mice (Fig. 1*A*). The blunted contraction-stimulated glucose transport in the MLKB1KO mice was not associated with a decreased ability of the muscles to generate force (Fig. S1*A*). Muscle weights were not different between groups (Fig. S1*B*), also suggesting that the muscle from the MLKB1KO mice was viable.

We also determined the effects of muscle-specific LKB1 knockout on contraction-stimulated glucose transport measured in vivo. For this purpose, anesthetized mice underwent 15 min of muscle contraction in situ, 2-deoxy-D-[^{3}H]-glucose was infused, and glucose transport into the tibialis anterior muscle was measured. Compared with controls, contraction-stimulated glucose transport was significantly impaired in MLKB1KO mice (Fig. 1*B*). Protein levels of GLUT4 and GLUT1, the major glucose transporters expressed in skeletal muscle, were not altered in the MLKB1KO mice (Fig. S1*C*). These data show that LKB1 is required for contraction-stimulated glucose transport in skeletal muscle.

To determine downstream signals involved in LKB1 signaling to glucose transport, we determined if the blunted contraction-stimulated glucose transport observed in the MLKB1KO mice was associated with a decrease in the phosphorylation of Akt substrate of 160 kDa (AS160/TBC1D4) and the AS160 paralog, TBC1D1. These Rab-GAP proteins are regulated by phosphorylation (29, 30), and overexpression of phosphorylation-defective mutants have been shown to impair contraction-stimulated glucose transport in skeletal muscle (31, 32). Phosphorylation of AS160 and TBC1D1 was detected using a phospho-Akt substrate (PAS) antibody that does not distinguish between AS160 and TBC1D1. In control mice, contraction significantly increased AS160/TBC1D1 PAS phosphorylation, an effect that was abolished in the MLKB1KO mice (Fig. 1*C*). In contrast, phosphorylation of ERK, another contraction-stimulated signaling protein that does not regulate glucose transport in skeletal muscle (33), was not altered in MLKB1KO mice (Fig. 1*D*). Thus, the lack of muscle LKB1 impaired phosphorylation of AS160/TBC1D1, critical downstream signals that are important for contraction-stimulated glucose transport.

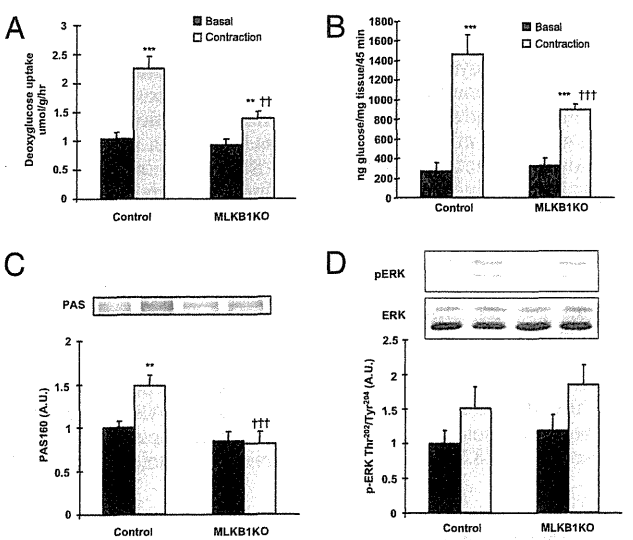

Fig. 1. Contraction-stimulated glucose transport is impaired in muscle-specific LKB1 knockout (MLKB1KO) mice. (*A*) Soleus muscles from MLKB1KO and littermate controls were contracted to measure glucose transport. (*B*) In vivo glucose transport was measured over the 15 min of contraction and the subsequent 30 min in tibialis anterior muscles. (*C* and *D*) Muscle lysates were obtained from gastrocnemius muscle, and PAS phosphorylation of AS160/TBC1D1 (*C*) and ERK phosphorylation (*D*) were determined by Western blot. Data are means ± SEM, n = 6/group for *A–C*, n = 5–12/group for *D*. $^{**}P < 0.01$ and $^{***}P < 0.001$ vs. basal of the same genotype. $^{\dagger\dagger}P < 0.01$ and $^{\dagger\dagger\dagger}P < 0.001$ vs. corresponding control.

ARK5/SNARK Activity Is Regulated by LKB1 and Muscle Contraction. Using the same methods described previously to measure glucose transport in vitro and in vivo for the MLKB1KO mice, we have shown normal rates of contraction-stimulated glucose transport in muscle-specific AMPKα2 inactive transgenic mice (20). Thus, the decrease in contraction-stimulated glucose transport in the MLKB1KO mice cannot be fully explained by lack of AMPKα2 activity. Therefore, we hypothesized that one or more additional AMPK-related protein kinases regulate contraction-stimulated glucose transport. In investigating the AMPK-related protein kinases, we found that ARK5/SNARK immune complex activity, using an antibody that does not differentiate between the two enzymes (34), was significantly decreased in muscles from MLKB1KO mice when measured in the basal state (Fig. 2*A*). Furthermore, contraction increased ARK5/SNARK activity by more than 2-fold in control littermates, whereas no increase was observed in the MLKB1KO mice (Fig. 2*A*). By immunoprecipitating muscle lysates with the ARK5/SNARK antibody and immunoblotting precipitates with the AMPKα2 antibody, we determined that there was no cross-reactivity between the ARK5/SNARK and AMPKα2 antibodies (Fig. S2). These findings raise the possibility that SNARK and/or ARK5 could be essential mediators of LKB1 in skeletal muscle.

Expression and Activity of SNARK in Mouse and Human Skeletal Muscle. Consistent with a previous report showing that contraction does not increase ARK5 activity in rat muscle (35), we found that in situ contraction did not increase ARK5 activity in our system in the mouse (Fig. S3*A*). We used direct DNA injection and electroporation to express wild-type ARK5 and mutant ARK5 ($Thr^{211}$to Ala) in tibialis anterior muscles of mice, which resulted in a 4.2-fold increase in ARK5 expression compared with endogenous ARK5 in empty vector controls. Overexpression of wild-type ARK5 and mutant ARK5 did not affect basal and contraction-stimulated glucose transport (Fig. S3*B*). Therefore, we focused on SNARK in subsequent experiments, and generated a polyclonal antibody that worked for immunoblotting and immunoprecipitation of SNARK and showed no cross-reactivity with ARK5 or AMPK (Fig. S4 *A–C*). Immunoblotting revealed that SNARK was expressed in multiple tissues, including liver, testis, kidney, brain, pancreas, heart ,and tibialis anterior muscle (Fig. 2*B*), and SNARK was also expressed in muscles composed of varying fiber types (Fig. 2*C*). Interestingly, the more oxidative muscles (red gastrocnemius and soleus), as well as heart (Fig. 2*B*), appeared to express two forms of SNARK (Fig. 2*C*). We also detected mRNA expression of SNARK in multiple tissues from the mouse, including skeletal muscle (Fig. 2*D*). Thus, SNARK is expressed in multiple muscles in the mouse.

Our initial experiment determined that contraction increased ARK5/SNARK in muscles from control mice but not MLKB1KO mice, so we next determined if contraction regulated SNARK activity independent of ARK5 by using the SNARK-specific antibody. Using this antibody in an immune complex assay, we found that contraction significantly increased SNARK activity in control mice, and the activity was significantly decreased in MLKB1KO

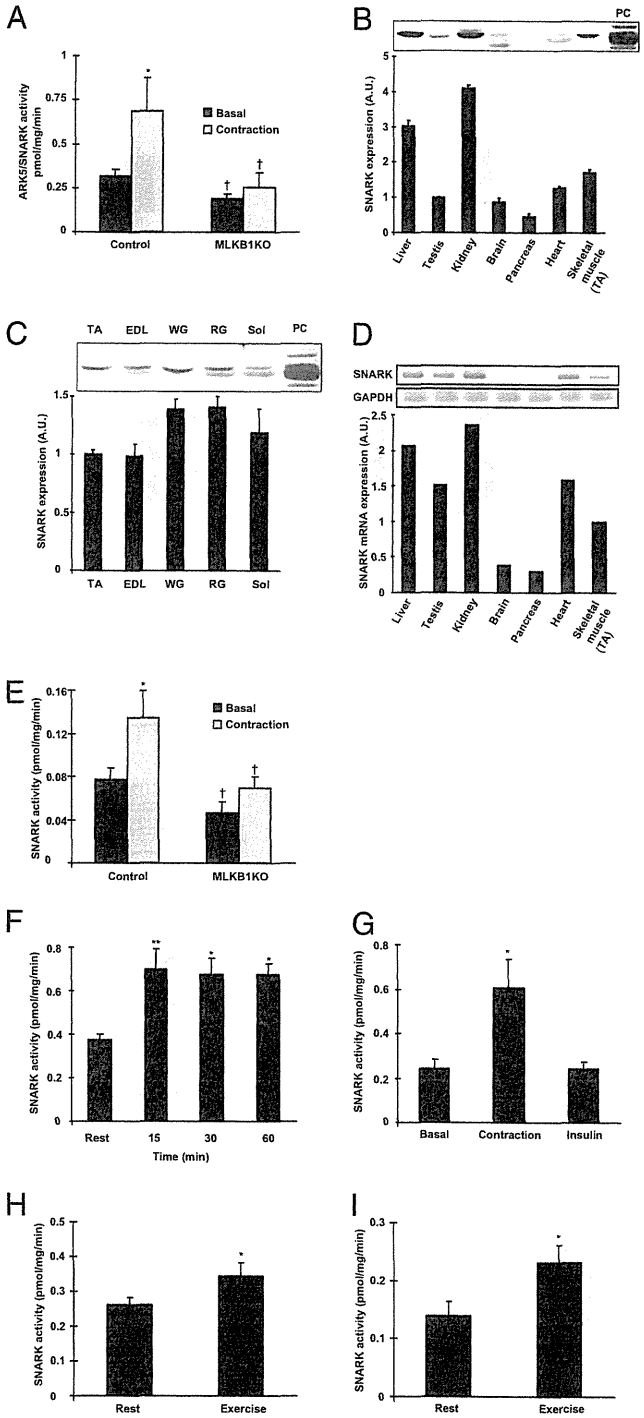

Fig. 2. SNARK expression and activity in mouse and human skeletal muscle. (*A*) Tibialis anterior muscles from MLKB1KO and littermate controls were contracted in situ for 15 min. ARK5/SNARK activity was measured using an immune complex assay with an antibody that recognizes both ARK5 and SNARK. Relative SNARK protein expression in various (*B*) mouse tissues and (*C*) mouse muscles (TA, tibialis anterior; EDL, extensor digitorum longus; WG, white gastrocnemius; RG, red gastrocnemius; SOL, soleus; PC, positive control). (*D*) Relative SNARK mRNA expression in various mouse tissues. (*E*) SNARK activity in tibialis anterior muscles from MLKB1KO and littermate controls was measured using an immune complex assay with SNARK antibody. (*F*) Time course of SNARK activity in tibialis anterior muscles from mice exercised on a treadmill at 22 m/min, 12% incline for 15, 30, and 60 min. (*G*) EDL muscles were isolated and incubated in KRB buffer. Muscles were either electrically stimulated to contract for 10 min or stimulated with insulin (50 mU/mL) for 40 min. (*H* and *I*) Healthy volunteers performed cycle exercise at 70% of peak work rate for 20 min (*H*) or 110% of peak work rate for 2 min (*I*). Data are means ± SEM, n = 5–11/group. $^{*}P < 0.05$ and $^{**}P < 0.01$ compared with control. $^{\dagger}P < 0.05$ vs. corresponding control.

mice (Fig. 2*E*). To determine if exercise in vivo increases SNARK activity in mouse skeletal muscle, mice were exercised on a rodent treadmill at a moderate intensity (22 m/min, 12% grade) for 15, 30, and 60 min. Immediately after exercise, tibialis anterior muscles were isolated, processed, and used for immune complex assays. SNARK activity was increased at all time points by approximately 2-fold above resting levels (Fig. 2*F*). Contraction of isolated extensor digitorum longus (EDL) muscles in vitro increased SNARK activity by 2.3-fold, whereas maximal insulin stimulation had no effect (Fig. 2*G*).

Immunoblotting lysates of vastus lateralis muscle from healthy human subjects revealed expression of SNARK in this tissue (Fig. S4*D*). Next, we determined whether SNARK activity is increased by acute exercise in human skeletal muscle. Healthy subjects exercised on a cycle ergometer at a moderate intensity (70% VO_{2max}) for 20 min or a high intensity (110% VO_{2max}) for 2 min, with muscle biopsies obtained before and immediately after the exercise. Both moderate and high-intensity exercise significantly increased SNARK activity (Fig. 2 *H* and *I*). These data suggest that LKB1 regulates SNARK activity in both mouse and human skeletal muscle.

Knockdown of SNARK Impairs Sorbitol-Induced Glucose Transport in C2C12 Cells. To determine whether SNARK mediates glucose transport in muscle cells, we generated C2C12 myotubes that were stably infected with retrovirus containing shRNA for SNARK as well as scrambled shRNA. SNARK protein was decreased by 73% in cells infected with shRNA for SNARK compared with the control cells infected with scrambled shRNA (Fig. 3*A*). SNARK is activated by high concentrations of sorbitol (25), which results in hyperosmolarity and an increase in glucose transport in rat skeletal muscle (36) and C2C12 cells (37). Furthermore, we have shown that similar to muscle contraction, sorbitol-stimulated glucose transport is not decreased in muscle-specific AMPKα2 inactive transgenic mice (20). Consistent with previous studies, sorbitol increased SNARK activity by 47% in C2C12 cells. We found that sorbitol increased glucose transport by 50% and that this increase was significantly impaired by knockdown of SNARK (Fig. 3*B*). Sorbitol-stimulated AMPK phosphorylation was not altered in both groups (Fig. 3*C*). SNARK knockdown did not affect insulin-stimulated glucose transport (Fig. 3*D*) or expression of the GLUT1 and GLUT4 glucose transporter proteins (Fig. S5 *A* and *B*). Thus, SNARK is necessary for sorbitol-induced glucose transport but not for insulin-stimulated glucose transport in C2C12 muscle cells.

Overexpression of Mutant SNARK in Tibialis Anterior Muscle Impairs Contraction-Stimulated Glucose Transport. To determine if SNARK regulates contraction-stimulated glucose transport in mouse skeletal muscle, we generated a mutant SNARK (mtSNARK) by replacing the LKB1 phosphorylation site, Thr, to Ala at amino acid 208. This mutation has been shown to inhibit its activity (16). We used direct DNA injection and electroporation to express mtSNARK in tibialis anterior muscles of mice and found that 10 d after injection there was a 2.5-fold increase in mtSNARK expression above endogenous SNARK (Fig. S6*A*). Expression of mtSNARK in muscle significantly decreased basal SNARK activity in the muscle and abolished the effect of contraction to increase SNARK activity (Fig. 4*A*), suggesting that the mutant worked as a dominant negative in skeletal muscle. There was no difference in the efficiency of the SNARK antibody to immunoprecipitate wild-type and mutant SNARK (Fig. S6*B*). Overexpression of mtSNARK did not alter SIK1 and MARK4 activities in mouse skeletal muscle (Fig. S6 *C* and *D*).

We expressed the mtSNARK construct in tibialis anterior muscles and measured glucose transport in vivo in response to 15

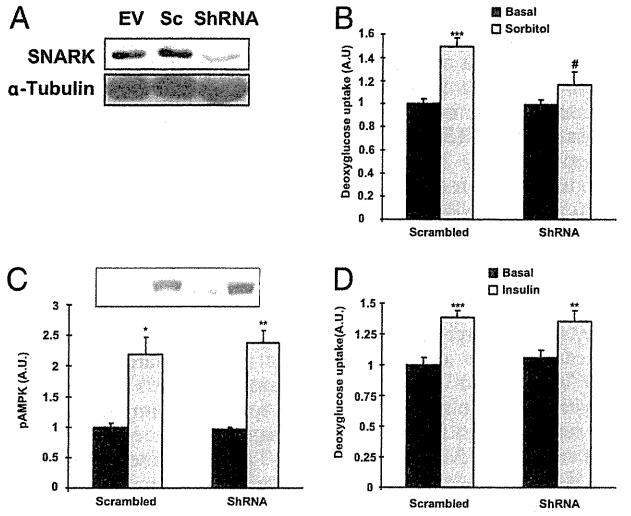

Fig. 3. Effects of SNARK inhibition in glucose transport in response to sorbitol and insulin. Retroviruses containing empty vector (EV), scrambled shRNA (Sc), and shRNA for SNARK (ShRNA) were infected in C2C12 cells. (*A*) SNARK expression was determined by immunoblot analysis. (*B* and *C*) Myotubes infected with Sc or ShRNA were incubated in the absence (black bars) or presence (grey bars) of sorbitol (300 mM) for 30 min. Glucose transport (*B*) and AMPK phosphorylation (*C*) were determined by 2-DG glucose transport measurement and Western blot analysis, respectively. (*D*) Cells were treated with insulin (100 nM) for 20 min and glucose transport was measured. $*P < 0.05$, $**P < 0.01$, and $***P < 0.001$ compared with control. $^{\dagger}P < 0.01$ vs. corresponding control.

min of in situ muscle contraction. Contraction increased glucose transport by 2.6-fold in empty vector injected muscles, whereas contraction-stimulated glucose transport was significantly impaired in muscles expressing mtSNARK (Fig. 4*B*). To determine if the combined inhibition of AMPKα2 and SNARK would further reduce contraction-stimulated glucose transport, we overexpressed mtSNARK in muscle-specific AMPKα2 inactive transgenic mice. There was no additive effect to inhibit contraction-stimulated glucose transport (Fig. S7).

Because contraction-stimulated PAS phosphorylation of AS160/TBC1D1 was abolished in MLKB1KO mice, we determined if expression of mtSNARK would impair AS160/TBC1D1 phosphorylation. Contraction-stimulated PAS phosphorylation of AS160/TBC1D1 was abolished in muscles overexpressing mtSNARK without altering expression of AS160 and TBC1D1 (Fig. 4*C*). This suggests that the inhibition of contraction-stimulated glucose transport with overexpression of mtSNARK is likely due, at least in part, to impaired phosphorylation of AS160 and TBC1D1.

The proximal molecular signaling mechanisms leading to contraction-stimulated glucose transport are known to be distinct from insulin signaling. Therefore, we hypothesized that SNARK signaling would not be essential for insulin-stimulated glucose transport. To test this hypothesis, insulin-stimulated glucose transport was measured by i.v. injection of a glucose bolus to stimulate a physiological insulin secretion (31). Consistent with the findings that knockdown of SNARK did not affect insulin-stimulated glucose transport in C2C12 cells (Fig. 3*D*), insulin-stimulated glucose transport was not altered by expression of the mtSNARK (Fig. 4*D*). These data suggest that SNARK is critical for contraction-stimulated, but not insulin-stimulated, glucose transport in the muscle.

To determine if changes in contraction-stimulated glucose transport by overexpression of mtSNARK might be due to a generalized dysfunction of muscle contraction, we measured several markers of normal muscle contraction. Overexpression of mtSNARK did not affect contraction-stimulated decreases in muscle glycogen (Fig. S8*A*). In addition, contraction-stimulated

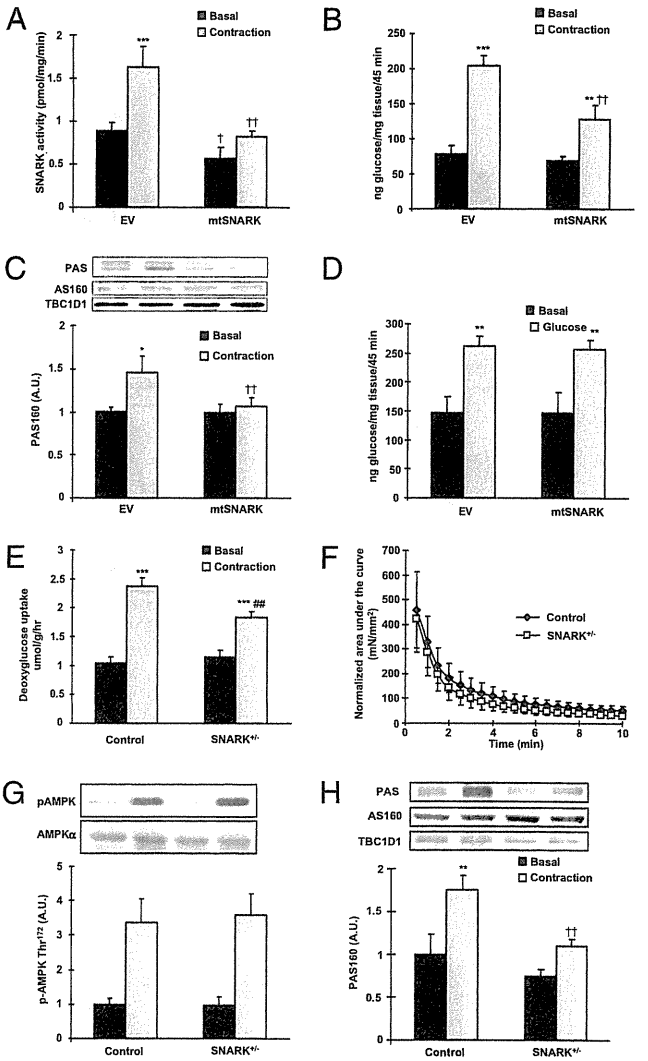

Fig. 4. Overexpression of mutant SNARK (mtSNARK) and knockdown of SNARK impaired contraction-stimulated glucose transport and phosphorylation of AS160 and TBC1D1. (*A–D*) mtSNARK replacing Thr^{208} to Ala was generated, and the cDNA construct was injected and electroporated into tibialis anterior muscles. Muscles were studied 10 d after injection. (*A*) SNARK activity was measured in tibialis anterior muscle lysates after 10 min of in situ contraction. (*B*) In vivo glucose transport in response to 15 min of in situ muscle contraction was measured in tibialis anterior muscles overexpressing either empty vector (EV) or mtSNARK. (*C*) Contraction-stimulated PAS phosphorylation of AS160 and TBC1D1 was measured by Western blot. Protein levels of AS160 and TBC1D1 were also determined by Western blot. (*D*) In vivo insulin-stimulated 2-DG glucose transport in skeletal muscle was measured by i.v. injection of a glucose bolus (1 mg/g). (*E*) Soleus muscles from SNARK $^{(+/-)}$ or control littermates were dissected and contracted in vitro for 10 min, and glucose transport was measured. (*F*) Force production was measured as described in Fig. S1*A*. (*G*) Contraction-stimulated AMPK Thr^{172} phosphorylation was determined by Western blot. (*H*) Contraction-stimulated phosphorylation of AS160 and TBC1D1 was determined by Western blot using PAS antibody. Data are means ± SEM, $n = 5–6$/group. $*P < 0.05$, $**P < 0.01$, and $***P < 0.001$ vs. basal in the same group. $^{\dagger}P < 0.05$ and $^{\dagger\dagger}P < 0.01$ vs. corresponding control.

AMPK and ERK phosphorylation, two signaling proteins activated in response to contraction, were also not altered by overexpression of mtSNARK (Fig. S8 *B* and *C*).

Contraction-Stimulated Glucose Transport Is Impaired in SNARK Heterozygotic Knockout $^{(+/-)}$ Mice. We studied glucose transport in whole-body SNARK knockout mice. Because homozygotic

SNARK knockout mice are embryonically lethal or abnormally developed (27), we used SNARK $^{(+/-)}$ mice. We confirmed that SNARK expression and activity were significantly reduced in the tibialis anterior muscles from SNARK $^{(+/-)}$ mice compared with wild-type littermates (Fig. S9 *A* and *B*). Mice were studied at 20 wk of age, a time point where there were no differences in body weights, blood glucose concentrations, and voluntary exercise capacity (Fig. S9 *C–E*). Soleus muscles were isolated and used to measure contraction-stimulated glucose transport in vitro. Contraction increased glucose transport in the muscles from both control and SNARK $^{(+/-)}$ mice, but contraction-stimulated glucose transport was significantly lower in the SNARK $^{(+/-)}$ mice (Fig. 4*E*). This impairment was not due to altered contraction force, because force production during contraction was normal in SNARK $^{(+/-)}$ mice (Fig. 4*F*). The SNARK $^{(+/-)}$ mice had normal stimulation of AMPK phosphorylation with contraction (Fig. 4*G*). Because overexpression of mtSNARK impaired contraction-stimulated PAS phosphorylation on AS160/TBC1D1, we assessed AS160/TBC1D1 PAS phosphorylation in SNARK $^{(+/-)}$ mice. Contraction-stimulated PAS phosphorylation was significantly impaired in SNARK $^{(+/-)}$ mice compared with control mice (Fig. 4*H*). Insulin-stimulated glucose transport was not altered in SNARK $^{(+/-)}$ mice (Fig. S9 *F* and *G*). Therefore, both overexpression of mtSNARK and heterozygotic knockout of SNARK inhibited glucose transport in response to contraction, and these decreases were associated with blunted AS160/TBC1D1 PAS phosphorylation.

Discussion

Given the benefits of exercise in the maintenance of glucose homeostasis, elucidating the mechanisms responsible for regulating contraction-stimulated glucose transport in skeletal muscle is an ongoing research challenge magnified by the increasing prevalence of type 2 diabetes. Though it has been known for many years that the underlying molecular signaling mechanisms regulating contraction- and insulin-stimulated glucose transport are distinct, the specific signals mediating the contraction effect have remained elusive. Our present findings suggest a role for the AMPK-related kinase SNARK in this process. This conclusion stems from studies of glucose transport using multiple model systems showing that (*i*) overexpression of mtSNARK in tibialis anterior muscle by electroporation decreased contraction-stimulated glucose transport; (*ii*) SNARK $^{(+/-)}$ mice had impaired contraction-stimulated glucose transport; (*iii*) deletion of LKB1 in skeletal muscle, which resulted in near ablation of SNARK activity, was associated with decreased contraction-stimulated glucose transport; (*iv*) knockdown of SNARK in C2C12 cells impaired sorbitol-stimulated glucose transport, a stimulus that has some similar characteristics to the effects on contraction in skeletal muscle; and (*v*) knockdown of SNARK and expression of mtSNARK did not decrease insulin-stimulated glucose transport, consistent with the concept of distinct intracellular signaling mechanisms for insulin- and contraction-stimulated glucose transport. In addition, we found that mtSNARK-expressing muscles and muscles from SNARK $^{(+/-)}$ mice had reduced contraction-stimulated phosphorylation of AS160/TBC1D1 on PAS sites, proteins critical in the regulation of contraction-stimulated glucose transport (31). Taken together, these data suggest that SNARK represents a unique signaling protein important in contraction-stimulated glucose transport in mouse skeletal muscle.

A role for SNARK in contraction-stimulated glucose transport is reasonable given recent indications that AMPK cannot be the sole signal mediating this metabolic function. A decade ago, the first evidence emerged that AMPK can mediate glucose transport in skeletal muscle (4, 11, 38), and subsequent studies using genetic models demonstrated that AICAR-mediated glucose transport and hypoxia, another potent stimulator of glucose transport in skeletal muscle, are both mediated by AMPKα2 (20–22). However, in investigating muscle contraction, genetic manipulation to decrease AMPK activity has been shown to partially decrease (22, 39, 40), not affect (20, 21, 41), or even increase (23) contraction-stimulated glucose transport. In contrast, in the current study we found that disruption of LKB1 in skeletal muscle results in impaired contraction-stimulated glucose transport, consistent with previous work investigating contraction-stimulated glucose transport in a hypomorphic LKB1 model (12). Because AMPKα2 inactive mice have normal contraction-stimulated glucose transport in our system (20), and MLKB1KO mice have ablated AMPKα2 activity, it is clear that the decrease in contraction-stimulated glucose transport in our MLKB1KO mice cannot be explained by the lack of AMPKα2 activity. We do not believe that AMPKα1 can explain the decrease in contraction-stimulated glucose transport in the MLKB1KO mice because AMPKα1 activity is not increased with this contraction protocol (13, 20). Taken together, these findings suggest that LKB1 is an important mediator of contraction-stimulated glucose transport in skeletal muscle and that one or more AMPK-related protein kinases are important in the regulation of contraction-stimulated glucose transport.

Little has been reported on the function of SNARK in various cells and tissues. SNARK induces tolerance of HepG2 cells to cell death by glucose starvation, and increases expression of anti-apoptotic genes in cancer cells, which can also lead to increased motility and invasiveness (42). The effects of SNARK deficiency on tumorigenesis of the large intestine has been investigated using SNARK $^{(+/-)}$ mice (27). Treatment with azoxymethane, a carcinogenic compound, increased aberrant crypt foci in SNARK $^{(+/-)}$ mice as compared with their wild-type counterparts, suggesting that the presence of SNARK helps to prevent early tumor development. A recent study of these SNARK $^{(+/-)}$ mice suggests that SNARK may also function in the control of metabolism (27). When treated with azoxymethane, SNARK $^{(+/-)}$ mice had increased body weights and increased fat mass and fatty livers, as well as increased serum triglyceride concentrations, hyperinsulinemia, hyperglycemia, and glucose intolerance. Although the function of SNARK in most tissues in the body is not known, it is possible that chronic impairment in contraction-stimulated glucose transport in skeletal muscle could be a major factor in the whole-body metabolic phenotype observed in the SNARK $^{(+/-)}$ mice.

We found that SNARK activity was increased by treadmill exercise, in situ contraction, and in vitro contraction in mouse skeletal muscles, and by cycle ergometer exercise in human vastus lateralis muscle. In contrast, we found no effect of insulin on SNARK activity in C2C12 muscle cells or incubated mouse muscle, which is in agreement with a recent study showing no effect of SNARK in insulin-stimulated glucose transport in human primary myotubes (28), and is also consistent with the well-established concept that the proximal signaling mechanisms leading to contraction- and insulin-stimulated glucose transport are distinct. Whereas insulin had no effect on SNARK activity, we have found that s.c. injection with AICAR (0.5 mg/g) increased SNARK activity in mouse skeletal muscle (Fig. S10*A*). This is consistent with previous studies showing that SNARK is activated by AICAR, AMP, glucose starvation, and oxidative stress in cultured cell lines (24–26, 43). The mechanism of SNARK activation with any stimuli and in all cell types has not been investigated extensively and therefore is not well understood. In vitro, LKB1 phosphorylates SNARK at Thr^{208}, increasing SNARK activity by 50-fold (16). Our MLKB1KO mice showed decreased SNARK activity, consistent with in vitro findings. Future studies will focus on understanding the mechanism of SNARK activation in skeletal muscle.

The present study clearly shows that LKB1 and SNARK are important molecules in the regulation of contraction-stimulated glucose transport. It is not apparent at this time if the reduced SNARK activity in the MLKB1KO mice mediates the reduced contraction-stimulated glucose transport in these animals. We attempted a rescue experiment of the MLKB1KO mice generating a constitutively active form of SNARK by mutating the LKB1 phosphorylation site, Thr to Glu at amino acid 208, and overexpressing it in the tibialis anterior muscle of the MLKB1KO mice. However, overexpression of the mutant in tibialis anterior muscle did not increase enzyme activity (Fig. S10*B*). Expression of wild-type SNARK increased SNARK activity 2-fold (Fig. S10*B*), similar to the effects of contraction. However, wild-type SNARK expression did not alter glucose transport in skeletal

muscle. It is possible that expression of wild-type SNARK is not sufficient to activate SNARK-mediated glucose transport in skeletal muscle, and other factors may need to work in unison with SNARK to increase glucose transport in skeletal muscle.

For many years, the signaling mechanisms by which exercise increases glucose transport in skeletal muscle have remained elusive. There is now strong evidence that multiple, or redundant, signals may mediate the effects of contraction on activating transport (18, 41). It is also now established that LKB1, independent from it effects on AMPKα2, functions to regulate contraction-stimulated glucose transport in response to muscle contraction. Moreover, we define SNARK as a contraction-activated signal involved in mediating glucose transport in skeletal muscle. In future studies it will be important to understand the mechanism of SNARK activation in vivo, as well as explore the possibility that SNARK mediates other aspects of metabolism in skeletal muscle.

Materials and Methods

Animals. Muscle-specific LKB1 knockout (MLKB1KO) mice were generated by Cre/loxP gene targeting as previously described (13). SNARK $^{(+/-)}$ mice have been described (27). Male mice were used for all experiments. All animal studies were in accordance with National Institutes of Health guidelines and approved by the Joslin Institutional Animal Care and Use Committee.

Statistical Analysis. Data are means ± SEM. All data were compared using Student's *t* test, paired *t* test, one-way ANOVA, or two-way ANOVA. The differences between groups were considered significant when $P < 0.05$.

For further information on human studies, cell culture, Western blot analysis, in vitro kinase assays, muscle incubation, treadmill exercise, and glucose transport measurement, see *SI Materials and Methods*.

ACKNOWLEDGMENTS. We thank Drs. R. A. DePinho and N. M. Bardeesy (Dana Farber Cancer Institute) for providing the floxed LKB1 mice, Dr. C. R. Kahn (Joslin Diabetes Center) for the MCK-Cre mice, Dr. J. Xie (Cell Signaling Technology, Danvers, MA) for generation of SNARK antibody, Yangfeng Lee for assistance with experiments, Julie A. Ripley for editorial contributions, and all other members of the Goodyear laboratory for critical discussions. This work was supported by National Institutes of Health Grants AR45670 and DK68626 (to L.J. G.), the Joslin Diabetes and Endocrinology Research Center Grant DK36836, Commission of the European Union Contract LSHM-CT-2004-005272 EXGENESIS, Lundbeck Foundation (to E.A.R.), and the Novo Nordisk Foundation, Copenhagen Muscle Research Centre, and the Danish Medical Research Council (J.F.P.W.). H.J. K. was supported by an American Physiological Society Fellowship in Physiological Genomics; T.T. was supported by a mentor-based fellowship awarded to L.J.G. from the American Diabetes Association; and S.J.L. was supported by an American Physiological Society Fellowship in Physiological Genomics.

1. Nesher R, Karl IE, Kipnis DM (1985) Dissociation of effects of insulin and contraction on glucose transport in rat epitrochlearis muscle. *Am J Physiol* 249:C226–C232.
2. Richter EA, Garetto LP, Goodman MN, Ruderman NB (1982) Muscle glucose metabolism following exercise in the rat: Increased sensitivity to insulin. *J Clin Invest* 69:785–793.
3. Wallberg-Henriksson H, Constable SH, Young DA, Holloszy JO (1988) Glucose transport into rat skeletal muscle: Interaction between exercise and insulin. *J Appl Physiol* 65:909–913.
4. Hayashi T, Hirshman MF, Kurth EJ, Winder WW, Goodyear LJ (1998) Evidence for 5′ AMP-activated protein kinase mediation of the effect of muscle contraction on glucose transport. *Diabetes* 47:1369–1373.
5. Lee AD, Hansen PA, Holloszy JO (1995) Wortmannin inhibits insulin-stimulated but not contraction-stimulated glucose transport activity in skeletal muscle. *FEBS Lett* 361:51–54.
6. Lund S, et al. (1998) Evidence against protein kinase B as a mediator of contraction-induced glucose transport and GLUT4 translocation in rat skeletal muscle. *FEBS Lett* 425:472–474.
7. Yeh JI, Gulve EA, Rameh L, Birnbaum MJ (1995) The effects of wortmannin on rat skeletal muscle. Dissociation of signaling pathways for insulin- and contraction-activated hexose transport. *J Biol Chem* 270:2107–2111.
8. Goodyear LJ, Giorgino F, Balon TW, Condorelli G, Smith RJ (1995) Effects of contractile activity on tyrosine phosphoproteins and PI 3-kinase activity in rat skeletal muscle. *Am J Physiol* 268:E987–E995.
9. Goodyear LJ, Kahn BB (1998) Exercise, glucose transport, and insulin sensitivity. *Annu Rev Med* 49:235–261.
10. Wojtaszewski JFP, Hansen BF, Ursø B, Richter EA (1996) Wortmannin inhibits both insulin- and contraction-stimulated glucose uptake and transport in rat skeletal muscle. *J Appl Physiol* 81:1501–1509.
11. Bergeron R, et al. (1999) Effect of AMPK activation on muscle glucose metabolism in conscious rats. *Am J Physiol* 276:E938–E944.
12. Sakamoto K, et al. (2005) Deficiency of LKB1 in skeletal muscle prevents AMPK activation and glucose uptake during contraction. *EMBO J* 24:1810–1820.
13. Koh HJ, et al. (2006) Skeletal muscle-selective knockout of LKB1 increases insulin sensitivity, improves glucose homeostasis, and decreases TRB3. *Mol Cell Biol* 26: 8217–8227.
14. Shaw RJ, et al. (2005) The kinase LKB1 mediates glucose homeostasis in liver and therapeutic effects of metformin. *Science* 310:1642–1646.
15. Jaleel M, et al. (2005) Identification of the sucrose non-fermenting related kinase SNRK, as a novel LKB1 substrate. *FEBS Lett* 579:1417–1423.
16. Lizcano JM, et al. (2004) LKB1 is a master kinase that activates 13 kinases of the AMPK subfamily, including MARK/PAR-1. *EMBO J* 23:833–843.
17. Hardie DG, Carling D, Carlson M (1998) The AMP-activated/SNF1 protein kinase subfamily: Metabolic sensors of the eukaryotic cell? *Annu Rev Biochem* 67:821–855.
18. Koh HJ, Brandauer J, Goodyear LJ (2008) LKB1 and AMPK and the regulation of skeletal muscle metabolism. *Curr Opin Clin Nutr Metab Care* 11:227–232.
19. Richter EA, Ruderman NB (2009) AMPK and the biochemistry of exercise: Implications for human health and disease. *Biochem J* 418:261–275.
20. Fujii N, et al. (2005) AMP-activated protein kinase alpha2 activity is not essential for contraction- and hyperosmolarity-induced glucose transport in skeletal muscle. *J Biol Chem* 280:39033–39041.
21. Jørgensen SB, et al. (2004) Knockout of the alpha2 but not alpha1 5′-AMP-activated protein kinase isoform abolishes 5-aminoimidazole-4-carboxamide-1-beta-4-ribofuranosidebut not contraction-induced glucose uptake in skeletal muscle. *J Biol Chem* 279:1070–1079.
22. Mu J, Brozinick JT, Jr, Valladares O, Bucan M, Birnbaum MJ (2001) A role for AMP-activated protein kinase in contraction- and hypoxia-regulated glucose transport in skeletal muscle. *Mol Cell* 7:1085–1094.
23. Maarbjerg SJ, et al. (2009) Genetic impairment of alpha2-AMPK signaling does not reduce muscle glucose uptake during treadmill exercise in mice. *Am J Physiol Endocrinol Metab* 297:1070–1079.
24. Lefebvre DL, et al. (2001) Identification and characterization of a novel sucrose-non-fermenting protein kinase/AMP-activated protein kinase-related protein kinase, SNARK. *Biochem J* 355:297–305.
25. Lefebvre DL, Rosen CF (2005) Regulation of SNARK activity in response to cellular stresses. *Biochim Biophys Acta* 1724:71–85.
26. Kuga W, et al. (2008) Nuclear localization of SNARK; its impact on gene expression. *Biochem Biophys Res Commun* 377:1062–1066.
27. Tsuchihara K, et al. (2008) Susceptibility of Snark-deficient mice to azoxymethane-induced colorectal tumorigenesis and the formation of aberrant crypt foci. *Cancer Sci* 99:677–682.
28. Rune A, Osler ME, Fritz T, Zierath JR (2009) Regulation of skeletal muscle sucrose, non-fermenting 1/AMP-activated protein kinase-related kinase (SNARK) by metabolic stress and diabetes. *Diabetologia* 52:2182–2189.
29. Sano H, et al. (2003) Insulin-stimulated phosphorylation of a Rab GTPase-activating protein regulates GLUT4 translocation. *J Biol Chem* 278:14599–14602.
30. Roach WG, Chavez JA, Mîinea CP, Lienhard GE (2007) Substrate specificity and effect on GLUT4 translocation of the Rab GTPase-activating protein Tbc1d1. *Biochem J* 403: 353–358.
31. Kramer HF, et al. (2006) AS160 regulates insulin- and contraction-stimulated glucose uptake in mouse skeletal muscle. *J Biol Chem* 281:31478–31485.
32. An D, et al. (2010) TBC1D1 regulates insulin- and contraction-induced glucose transport in mouse skeletal muscle. *Diabetes* 59:1358–1365.
33. Hayashi T, Hirshman MF, Dufresne SD, Goodyear LJ (1999) Skeletal muscle contractile activity in vitro stimulates mitogen-activated protein kinase signaling. *Am J Physiol* 277:C701–C707.
34. Suzuki A, et al. (2003) Identification of a novel protein kinase mediating Akt survival signaling to the ATM protein. *J Biol Chem* 278:48–53.
35. Fisher JS, et al. (2005) Muscle contractions, AICAR, and insulin cause phosphorylation of an AMPK-related kinase. *Am J Physiol Endocrinol Metab* 289:E986–E992.
36. Hayashi T, et al. (2000) Metabolic stress and altered glucose transport: Activation of AMP-activated protein kinase as a unifying coupling mechanism. *Diabetes* 49: 527–531.
37. Fryer LG, et al. (2002) Characterization of the role of the AMP-activated protein kinase in the stimulation of glucose transport in skeletal muscle cells. *Biochem J* 363: 167–174.
38. Kurth-Kraczek EJ, Hirshman MF, Goodyear LJ, Winder WW (1999) 5′ AMP-activated protein kinase activation causes GLUT4 translocation in skeletal muscle. *Diabetes* 48: 1667–1671.
39. Jensen TE, et al. (2007) Possible CaMKK-dependent regulation of AMPK phosphorylation and glucose uptake at the onset of mild tetanic skeletal muscle contraction. *Am J Physiol Endocrinol Metab* 292:E1308–E1317.
40. Lefort N, St-Amand E, Morasse S, Côté CH, Marette A (2008) The alpha-subunit of AMPK is essential for submaximal contraction-mediated glucose transport in skeletal muscle in vitro. *Am J Physiol Endocrinol Metab* 295:E1447–E1454.
41. Jensen TE, Wojtaszewski JF, Richter EA (2009) AMP-activated protein kinase in contraction-regulation of skeletal muscle metabolism: Necessary and/or sufficient? *Acta Physiol (Oxf)* 196:155–174.
42. Suzuki A, et al. (2003) Induction of cell-cell detachment during glucose starvation through F-actin conversion by SNARK, the fourth member of the AMP-activated protein kinase catalytic subunit family. *Biochem Biophys Res Commun* 311:156–161.
43. Hurov JB, et al. (2007) Loss of the Par-1b/MARK2 polarity kinase leads to increased metabolic rate, decreased adiposity, and insulin hypersensitivity in vivo. *Proc Natl Acad Sci USA* 104:5680–5685.

Ann. N.Y. Acad. Sci. ISSN 0077-8923

ANNALS OF THE NEW YORK ACADEMY OF SCIENCES
Issue: *Mitochondrial Research in Translational Medicine*

The NADH-fumarate reductase system, a novel mitochondrial energy metabolism, is a new target for anticancer therapy in tumor microenvironments

Eriko Tomitsuka,[1,2] Kiyoshi Kita,[2] and Hiroyasu Esumi[1]

[1]Investigative Treatment Division, Research Center for Innovative Oncology, National Cancer Center Hospital East, Chiba, Japan. [2]Department of Biomedical Chemistry, Graduate School of Medicine, The University of Tokyo, Tokyo, Japan

Address for correspondence: Eriko Tomitsuka, Investigative Treatment Division, Research Center for Innovative Oncology, National Cancer Center Hospital East, 6-5-1 Kashiwanoha, Kashiwa, Chiba 277-8577, Japan. etomitsu@east.ncc.go.jp

Since deficiencies of critical nutrients and hypoxia are observed in hypovascular tumors, glycolysis alone cannot explain how cancer cells maintain their required energy levels. To study energy metabolism in cancer cells within such tumor microenvironments, we examined the NADH-fumarate reductase system, which is found in anaerobic organisms, such as parasitic helminthes. In human cancer cells cultured under tumor microenvironment-mimicking conditions, mitochondrial NADH-fumarate reductase activity increased in parallel with an increase in fumarate reductase activity, which is the reverse reaction of succinate-ubiquinone reductase and is regulated by the phosphorylation of its subunit. Pyrvinium pamoate, an anthelmintic drug, has an anticancer effect within tumor-mimicking microenvironments. We found that one of the biological mechanisms of pyrvinium is the inhibition of the NADH-fumarate reductase system. Therefore, the NADH-fumarate reductase system might be important for maintaining mitochondrial energy metabolism within the tumor microenvironments and might represent a novel target for anticancer therapies.

Keywords: complex II; energy metabolism; mitochondria; phosphorylation; tumor microenvironment

Introduction

Cancer cells live in various environments under conditions of both sufficient and inadequate nutrition and oxygen. In normal cells, where adequate oxygen is supplied to tissues, adenosine 5′-triphosphate (ATP) is mainly synthesized by oxidative phosphorylation in mitochondria. Under conditions of abundant blood vessel formation, cancer cells are known to generate ATP mainly by glycolysis, as observed by the increase in glucose uptake and lactate production, known as the Warburg effect.[1] On the other hand, in hypovascular tumors, such as pancreatic cancer, deficiencies in both nutrients and oxygen are observed because of the limited blood supply to the tumor tissues. In normal tissues, the oxygen concentration is almost stable; in tumor tissues, however, the oxygen concentrations are relatively low and sometimes extremely low.[2] Moreover, the glucose concentrations are also lower in some tumor tissues than in normal tissues.[3] Under hypoxic conditions, an increase in glycolysis has been the principal explanation for how cancer cells transduce energy.[1] However, because some cancer cells do not exhibit a high glycolytic activity[4] and as the amount of glucose is limited in hypovascular tumors, glycolysis alone cannot explain how cancer cells maintain their required energy levels under such conditions.

When the tumor microenvironments are mimicked by withholding nutrients and oxygen, cancer cells become resistant to conventional chemotherapies. Conventional anticancer drugs, such as 5-FU and cisplatin, reportedly exert cytotoxic effects in normal medium but only have a minimal effect in nutrient-deprived medium.[5] Under hypoxic conditions, cancer cells become resistant to some anticancer drugs, such as bleomycin and vincristine.[6]

doi: 10.1111/j.1749-6632.2010.05620.x

Ann. N.Y. Acad. Sci. 1201 (2010) 44–49

These data show that these anticancer drugs are not effective in cancer cells under tumor microenvironmental conditions. Therefore, new anticancer therapies that are effective against cancer cells exposed to tumor microenvironmental conditions are needed.

Energy metabolism in cancer cells under tumor microenvironmental conditions

Despite the occurrence of hypoxia and the limited glucose concentrations in tumor tissues under tumor microenvironmental conditions, the accumulation of amino acids, thought to result from the autophagic degradation of proteins, has been observed.[3] Therefore, cancer cells in the tumor microenvironments can use amino acids for ATP synthesis instead of glucose. We became interested in anaerobic respiration, specifically the reduced nicontinamide adenine dinucleotide (NADH)-fumarate reductase system, which exists in anaerobic organisms, such as parasitic helminthes.[7] This system is observed not only in ascarids but also in many parasites, suggesting that it is a common environmental adaptation enabling energy metabolism.[8] In the aerobic respiratory chain in mammalian mitochondria, electrons from the tricarboxylic acid (TCA) cycle pass via complex I (NADH-ubiquinone reductase) -> complex III (ubiquinol-cytochrome *c* reductase) -> complex IV (cytochrome *c* oxidase), or via complex II (succinate-ubiquinone reductase) -> complex III -> complex IV. Complex I, complex III, and complex IV function as proton pumps and generate a proton gradient, which is the driving force of ATP synthesis by complex V (ATP synthase) (Fig. 1A). On the other hand, the NADH-fumarate reductase system is only composed of complex I and the reverse reaction of complex II, forming an anaerobic electron transport system in mitochondria; this system results in succinate formation via the fumarate reductase (FRD) activity in complex II. This system does not need oxygen, and only complex I functions as a proton pump, forming a transmembrane electrochemical proton gradient for ATP synthesis through complex V (Fig. 1B). Moreover, in the NADH-fumarate reductase system, amino acids can be used instead of glucose, e.g., aspartate -> oxaloacetate -> malate -> fumarate.[9] However, whether this system exists and functions in mammals has received minimal investigation.

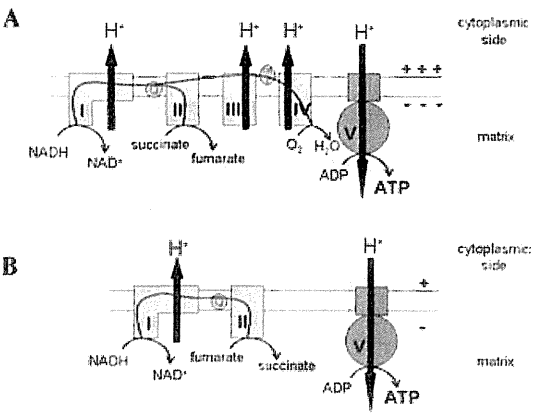

Figure 1. Mitochondrial respiratory chains. (A) Oxidative phosphorylation system. Under normoxic conditions in mammalian mitochondria, electrons from the TCA cycle pass through complex I (NADH-ubiquinone reductase) to ubiquinone, complex III (ubiquinol-cytochrome *c* reductase), cytochrome *c*, and complex IV (cytochrome *c* oxidase) or through complex II (succinate-ubiquinone reductase) to ubiquinone, complex III, cytochrome *c*, and complex IV. At the same time, complex I, complex III, and complex IV function as proton pumps to generate a proton gradient, driving complex V (ATP synthase). (B) NADH-fumarate reductase system. Under hypoxic conditions in *Ascaris suum* mitochondria and under tumor microenvironmental conditions, such as the nutrient-starved, hypoxic conditions in the mitochondria of cancer cells, electrons pass through complex I, and the reverse reaction of complex II (fumarate reductase). Only complex I functions as a proton pump, generating a proton gradient and driving complex V even in the absence of oxygen.

As a first step to understanding energy metabolism in cancer cells under nutrition-starved and hypoxic conditions and to determining whether the NADH-fumarate reductase system is active in human mitochondria, we measured the mitochondrial NADH-fumarate reductase activity in human cancer cells cultured under a variety of conditions. Cancer cells cultured under ordinary conditions had a relatively low NADH-fumarate reductase activity, but the activity level increased when the cells were cultured under tumor microenvironment-mimicking conditions where both oxygen and glucose were deprived. In HepG2 hepatocellular carcinoma cells, the NADH-fumarate reductase activity level was 1.7 ± 0.2 nmol/min/mg proteins under normal conditions and 3.8 ± 0.8 nmol/min/mg proteins after 5 days of tumor-mimicking microenvironmental conditions, although the activity lower than previously reported data and our data for bovine mitochondria (12 nmol/min/mg proteins,[10] 8.5 ± 1.9 nmol/min/mg proteins; E. Tomitsuka et al.,

unpublished observations). On the other hand, the NADH-oxidase activity level, which consists of aerobic respiratory chain enzyme complex I-III-IV activity, decreased and ultimately disappeared under such conditions (E. Tomitsuka et al., unpublished observations). Therefore, NADH-fumarate reductase appears to be the main functional respiratory chain under tumor microenvironmental conditions in cancer cells.

Next, to determine how the NADH-fumarate reductase system functions in mitochondria, especially with regard to ATP synthesis, we analyzed whether this system can generate a mitochondrial membrane potential capable of driving ATP synthesis through ATP synthase. To detect the mitochondrial membrane potentials, the quenching of Rhodamine 123 fluorescence was measured.[11] When succinate, which is an succinate-ubiquinone reductase (SQR) substrate, was added to fresh mitochondria from cancer cells, a mitochondrial membrane potential was generated. When cyanide, which is a complex IV inhibitor, was added, the membrane potential decreased. Similarly, when fumarate, which is an NADH-fumarate reductase substrate, was added to fresh mitochondria from cancer cells cultured under glucose-deprived and hypoxic conditions, a mitochondrial membrane potential was generated. When cyanide was added, however, the membrane potential did not decrease [Tomitsuka, 2010; submitted for publication]. These data suggest that the NADH-fumarate reductase system is active and can generate a mitochondrial membrane potential capable of driving ATP synthesis through ATP synthase (Fig. 1B). Therefore, the NADH-fumarate reductase system might have a major role in ATP generation under tumor microenvironmental conditions.

Functional change in complex II under tumor microenvironmental conditions

One of the major changes between the normoxic respiratory chain and the NADH-fumarate reductase system is the function of complex II. In the normoxic respiratory chain, complex II functions as SQR and forms fumarate. Under hypoxic and glucose-deprived conditions, however, complex II functions as FRD in the NADH-fumarate reductase system and forms succinate. In mammalian cells, the accumulation of succinate under hypoxic conditions has been reported, and complex II has been suggested to function as FRD.[12] In cancer cells under glucose-deprived and hypoxic conditions, the FRD activity increased, whereas the SQR activity slightly decreased.[13] Because the NADH-fumarate reductase activities also increased under these conditions, the increase in NADH-fumarate reductase activity might be related to a change in the function of complex II. Complex II consists of four subunits, and the Flavoprotein subunit (Fp), which contains the site of succinate/fumarate conversion, has been shown to be a phosphoprotein.[14,15] In complex I of bovine mitochondria, the phosphorylation of the 18-kDa iron-protein fraction subunit by a cAMP-dependent protein kinase has been reported, and the activity of complex I is regulated by its phosphorylation status.[16] In complex IV, the phosphorylation of subunits I, II, and Vb has been reported, and the activity of complex IV is also regulated by its phosphorylation status.[17] However, the relationship between the phosphorylation status of Fp and the function of complex II had not been reported. We investigated whether the SQR and FRD activities were regulated by the phosphorylation of Fp. First, the activities of complex II after treatment with phosphatase and protein kinase were measured. After phosphatase treatment, the SQR activity increased and the FRD activity decreased in a dose-dependent manner. Meanwhile, after treatment with protein kinase, the SQR activity decreased and the FRD activity increased. Using two-dimensional gel electrophoresis, the Fp proteins were separated with different pI values equivalent to the phosphorylation status. The quantity of dephosphorylated Fp increased after phosphatase treatment, whereas the quantity of dephosphorylated Fp decreased after treatment with protein kinase. These data are consistent with the idea that a low-phosphorylation status of the Fp subunit results in a higher SQR activity and a lower FRD activity.[13] Therefore, the change of the normoxic respiratory chain to the NADH-fumarate reductase system might be related to functional changes in complex II that are regulated by the phosphorylation of the Fp subunit.

Development of anticancer agents effective against cancer cells under tumor microenvironmental conditions

Previously, we reported several effective anticancer agents that exert cytotoxic effects on cancer cells under nutrient-deprived conditions mimicking the tumor microenvironments. Kigamicin D and

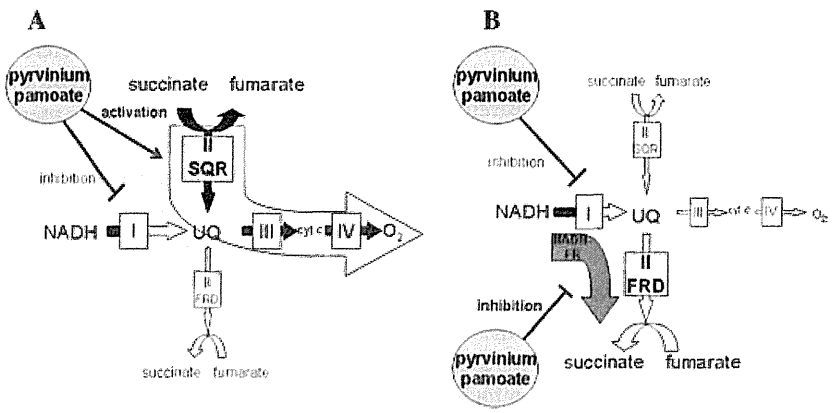

Figure 2. Effects of pyrvinium pamoate on respiratory chains under normal conditions and tumor microenvironmental conditions. (A) Under normal conditions, pyrvinium pamoate activates complex II activity (SQR) and inhibits complex I activity. Pyrvinium pamoate activates the mitochondrial respiratory chain via complex II, despite inhibiting complex I. (B) Under tumor microenvironmental conditions, pyrvinium pamoate inhibits the NADH-fumarate reductase system (NADH-FR) but does not activate complex II (SQR). Therefore, pyrvinium pamoate inhibits both respiratory chains.

arctigenin had a highly cytotoxic effect against cancer cells within a nutrient-deprived medium as well as exhibiting antitumor activities.[5,18] Pyrvinium pamoate, an anthelmintic, has also been reported to act as an anticancer compound in human cancer cells under tumor-mimicking microenvironmental conditions.[19] Parasitic helminthes live in the intestines of their hosts, where the oxygen concentration is relatively low, and they use the phosphoenolpyruvate carboxykinase (PEPCK)-succinate pathway for anaerobic energy production. The final step in this pathway is the NADH-fumarate reductase system.[7] Pyrvinium pamoate is used as an anthelmintic for pinworm infections; this compound is reportedly active within the gastrointestinal tract without being absorbed, and a single dose of 5 mg/kg body weight is highly effective.[20] The inhibitory effect of pyrvinium pamoate on pinworms is thought to occur via a mechanism that interferes with glucose absorption and the inhibition of FRD activity.[21] Although another anthelmintic, tetramisole, reportedly inhibits FRD activity in *Ascaris suum* and *Haemonchus contortus*,[22] no direct evidence has been reported on the inhibition of FRD activity by pyrvinium pamoate. To confirm whether pyrvinium pamoate inhibits NADH-fumarate reductase activity in parasites, we examined the effect of pyrvinium pamoate on respiratory chain enzyme activities in *A. suum*. Interestingly, pyrvinium pamoate inhibited not only complex II activity but also complex I activity, both of which are involved in the NADH-fumarate reductase system in *A. suum* mitochondria. Likewise, pyrvinium pamoate also inhibited NADH-fumarate reductase activity in mammalian mitochondria. Moreover, pyrvinium pamoate enhanced the SQR activity of complex II in mammalian mitochondria. The activation of complex II by pyrvinium pamoate is quite different feature from complex II in parasites. However, in cancer cells under hypoxic and glucose-deprived conditions, the activation of SQR by pyrvinium pamoate disappeared and NADH-fumarate reductase activity was inhibited. Then, to determine whether pyrvinium pamoate affects mitochondrial functions, the mitochondrial membrane potentials were measured. Pyrvinium pamoate inhibited the mitochondrial membrane potential generated by fumarate but did not affect the membrane potential generated by succinate. These data suggest that pyrvinium pamoate affects mitochondrial dysfunction via the inhibition of the NADH-fumarate reductase system, possibly affecting the generation of ATP [Tomitsuka 2010; submitted for publication]. The cytotoxic effects of pyrvinium pamoate on cancer cells differ according to the environmental conditions.[19] Our data suggest that under normal conditions, pyrvinium is not cytotoxic because of the enhancement of SQR activity, even if complex I is inhibited (Fig. 2A). Under hypoxic and glucose-deprived conditions mimicking the tumor microenvironments, however, pyrvinium pamoate inhibits the

NADH-fumarate reductase system in the hypoxic respiratory chain, and the pyrvinium pamoate-induced activation of the SQR activity of complex II in the normoxic respiratory chain disappears. Consequently, pyrvinium pamoate becomes cytotoxic to cancer cells under tumor microenvironmental conditions (Fig. 2B).

Recently, some effects of pyrvinium on gene transcription induced by glucose starvation and the inhibition of the androgen receptor have been reported.[23,24] We previously reported that pyrvinium pamoate suppressed protein kinase B (PKB)/Akt activation under glucose-deprived conditions, suggesting that pyrvinium pamoate affects the PKB/Akt signaling pathway.[19] As described in the previous section, the phosphorylation of the Fp subunit in complex II regulates its activities, and the dephosphorylation of Fp increased SQR activity after phosphatase treatment. We speculated that the effects of pyrvinium pamoate are also related to the phosphorylation of its Fp subunit, because pyrvinium pamoate enhanced the SQR activity of complex II under normal conditions, similar to the effect of phosphatase on SQR activity. When examined using two-dimensional gel electrophoresis, pyrvinium pamoate treatment increased the amount of dephosphorylated Fp; furthermore, treatment with pyrvinium pamoate plus phosphatase enhanced the increase in dephosphorylated Fp. Next, to clarify the relations of the effects of phosphatase and pyrvinium pamoate on SQR activity, we examined whether phosphatase inhibitors would inhibit the effect of pyrvinium pamoate on SQR activity. Treatment with phosphatase inhibitors plus pyrvinium did not enhance SQR activity. Therefore, these data suggest that the effect of pyrvinium pamoate on SQR activity is related to the effect of phosphatases and that pyrvinium pamoate might enhance SQR activity through the activation of mitochondrial phosphatase(s) [Tomitsuka 2010; submitted for publication]. Although kinases and phosphatases have been detected in mitochondria, the details of their physiological roles are poorly understood.[25] The regulation of complex II activities via phosphatases and kinases remains poorly understood. In a database analysis, the Fp sequence exhibited several phosphorylation motifs including cAMP-dependent protein kinase motifs, and Salvi reported that Fgr tyrosine kinase, a member of the Src kinase family, phosphorylated the Fp subunit.[15] The phosphatase that is the actual target of pyrvinium pamoate remains to be identified.

Conclusion

The NADH-fumarate reductase system is important for maintaining mitochondrial function within the tumor microenvironments. Pyrvinium pamoate is a good leading compound for the development of tumor microenvironments-specific anticancer reagents. Thus, the NADH-fumarate reductase system should be regarded as a novel target for anticancer therapy.

Acknowledgments

This work was supported in part by a Research Resident Fellowship award from the Foundation for the Promotion of Cancer Research (Japan) of the 3rd Term Comprehensive 10-Year Strategy for Cancer Control, and by a Grant-in-Aid for Creative Scientific Research (18GS0314) from the Japan Society for the Promotion of Science, and for Scientific Research on Priority Areas (18073004) and Targeted Proteins Research Program from the Ministry of Education, Culture, Sports, Science and Technology, Japan.

Conflicts of interest

The authors declare no conflicts of interest.

References

1. Warburg, O. 1956. On respiratory impairment in cancer cells. *Science* **124:** 269–270.
2. Brown, J.M. & W.R. Wilson. 2004. Exploiting tumour hypoxia in cancer treatment. *Nat. Rev. Cancer* **4:** 437–447.
3. Hirayama, A. *et al.* 2009. Quantitative metabolome profiling of colon and stomach cancer microenvironment by capillary electrophoresis time-of-flight mass spectrometry. *Cancer Res.* **69:** 4918–4925.
4. Zu, X.L. & M. Guppy. 2004. Cancer metabolism: facts, fantasy, and fiction. *Biochem. Biophys. Res. Comm.* **313:** 459–465.
5. Lu, J. *et al.* 2004. Kigamicin D, a novel anticancer agent based on a new anti-austerity strategy targeting cancer cell's tolerance to nutrient starvation. *Cancer Sci.* **95:** 547–552.
6. Teicher, B.A., J.S. Lazo & A.C. Sartorelli. 1981. Classification of antineoplastic agents by their selective toxicities toward oxygenated and hypoxic tumor cells. *Cancer Res.* **41:** 73–81.
7. Kita, K. *et al.* 2002. Role of complex II in anaerobic respiration of the parasite mitochondria from *Ascaris suum* and *Plasmodium falciparum*. *Biochim. Biophys. Acta* **1553:** 123–139.
8. Matsumoto, J. *et al.* 2008. Anaerobic NADH-fumarate reductase system is predominant in the respiratory chain of *Echinococcus multilocularis*, providing a novel target for the

chemotherapy of alveolar echinococcosis. *Antimicrob. Agents Chemother.* **52:** 164–170.
9. Pisarenko, O. *et al.* 1988. An assessment of anaerobic metabolism during ischemia and reperfusion in isolated guinea pig heart. *Biochim. Biophys. Acta* **934:** 55–63.
10. Galkin, A. *et al.* 2009. Lack of oxygen deactivates mitochondrial complex I: implications for ischemic injury? *J. Biol. Chem.* **284:** 36055–36061.
11. Esposti, M.D. 2001. Assessing functional integrity of mitochondria in vitro and in vivo. *Methods Cell Biol.* **65:** 75–96.
12. Weinberg, J.M. *et al.* 2000. Mitochondrial dysfunction during hypoxia/reoxygenation and its correction by anaerobic metabolism of citric acid cycle intermediate. *Proc. Natl. Acad. Sci. USA* **97:** 2826–2831.
13. Tomitsuka, E., K. Kita & H. Esumi. 2009. Regulation of succinate-ubiquinone reductase and fumarate reductase activities in human complex II by phosphorylation of its flavoprotein subunit. *Proc. Jpn. Acad., Ser. B. Phys. Biol. Sci.* **85:** 258–265.
14. Schulenberg, B. *et al.* 2003. Analysis of steady-state protein phosphorylation in mitochondria using novel fluorescent phosphosensor dye. *J. Biol. Chem.* **278:** 27251–27255.
15. Salvi, M. *et al.* 2007. Identification of the flavoprotein of succinate dehydrogenase and aconitase as *in vitro* mitochondrial substrates of Fgr tyrosine kinase. *FEBS Lett.* **581:** 5579–5585.
16. Papa, S. *et al.* 2002. The NADH: ubiquinone oxidoredactase (Complex I) of the mammalian respiratory chain and the cAMP cascade. *J. Bioenerg. Biomembr.* **34:** 1–10.
17. Lee, I., E. Bender & B. Kadenbach. 2002. Control of mitochondrial membrane potential and ROS formation by reversible phosphorylation of cytochrome *c* oxidase. *Mol. Cell Biochem.* **234/235:** 63–70.
18. Awale, S. *et al.* 2006. Identification of arctigenin as an antitumor agent having the ability to eliminate the tolerance of cancer cells to nutrient starvation. *Cancer Res.* **66:** 1751–1757.
19. Esumi, H. *et al.* 2004. Antitumor activity of pyrvinium pamoate, 6-(dimethylamino)-2-[2-(2,5-dimethyl-1-phenyl-1H-pyrrol-3-yl)ethenyl]-1-methyl-quinolinium pamoate salt, showing preferential cytotoxicity during glucose starvation. *Cancer Cell* **95:** 685–690.
20. Buchanan, R.A. *et al.* 1974. Pyrvinium pamoate. *Clin. Pharmacol. Ther.* **16:** 716–719.
21. Sheth, U.K. 1975. Mechanisms of anthelmintic action. *Prog. Drug Res.* **19:** 147–157.
22. Bossche, H.V. D. 1972. *Biochemical Effects of Tetramisole: Comparative Biochemistry of Parasites*: 117–125. Academic Press. New York.
23. Yu, D.H. *et al.* 2008. Pyrvinium targets the unfolded protein response to hypoglycemia and its anti-tumor activity is enhanced by combination therapy. *PLoS One* **3:** e3951.
24. Jones, J.O. *et al.* 2009. Non-competitive androgen receptor inhibition in vitro and in vivo. *Proc. Natl. Acad. Sci.* **106:** 7233–7238.
25. Pagliarini, D.J. & J.E. Dixon 2006. Mitochondrial modulation: reversible phosphorylation takes center stage? *Trends Biochem. Sci.* **31:** 26–34.